THE JOURNAL OF
PHYSICAL CHEMISTRY C

pubs.acs.org/JPCC

Article

Electrochemically Controlled Ion Dynamics in Porphyrin Nanostructures

Andrés F. Molina-Osorio, José A. Manzanares, Alonso Gamero-Quijano, and Micheál D. Scanlon*

Cite This: *J. Phys. Chem. C* 2020, 124, 18346−18355

Read Online

ACCESS | Metrics & More | Article Recommendations | Supporting Information

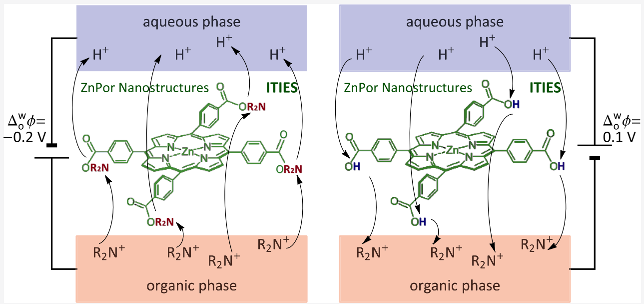

ABSTRACT: The dynamics of ion intercalation into solid matrices influences the performance of key components in most energy storage devices (Li-ion batteries, supercapacitors, fuel cells, etc.). Electrochemical methods provide key information on the thermodynamics and kinetics of these ion-transfer processes but are restricted to matrices supported on electronically conductive substrates. In this article, the electrified liquid|liquid interface is introduced as an ideal platform to probe the thermodynamics and kinetics of reversible ion intercalation with nonelectronically active matrices. Zinc(II) meso-tetrakis(4-carboxyphenyl)porphyrin nanostructures were self-assembled into floating films of ordered nanostructures at the water|α,α,α-trifluorotoluene interface. Electrochemically polarizing the aqueous phase negatively with respect to the organic phase led to organic ammonium cations intercalating into the zinc porphyrin nanostructures by binding to anionic carboxyl sites and displacing protons through ion exchange at neutral carboxyl sites. The cyclic voltammograms suggested a positive cooperativity mechanism for ion intercalation linked with structural rearrangements of the porphyrins within the nanostructures and were modeled using a Frumkin isotherm. The model also provided a robust understanding of the dependence of the voltammetry on the pH and organic electrolyte concentration. Kinetic analysis was performed using potential step chronoamperometry, with the current transients composed of "adsorption" and nucleation components. The latter were associated with domains within the nanostructures where, due to structural rearrangements, ion binding and exchange took place faster. This work opens opportunities to study the thermodynamics and kinetics of purely ionic ion intercalation reactions (not induced by redox reactions) in floating solid matrices using any desired electrochemical method.

INTRODUCTION

Charge transfer reactions at electrified interfaces critically influence the performance of devices with energy-related applications.[1,2] The continuous development of sustainable technologies relies on a precise analysis of the thermodynamics and kinetics underlying the charge transfer reactions involved.[3] Of the different charge transfer phenomena, a molecular-scale understanding of electron transfer across solid|liquid interfaces is now accessible.[4] However, such an in-depth analysis remains a challenge for interfacial ion transfer between two different phases.

Ion-transfer reactions are of major importance in many energy storage technologies. A key step during the cycling of lithium-ion (Li-ion) batteries is the reversible ion transfer, termed intercalation and deintercalation, of Li$^+$ between the electrolyte and the cathode material.[4] For supercapacitor applications, conducting polymers exhibit pseudocapacitance through doping and dedoping of the polymer backbone, which involves intercalation and deintercalation of the electrolyte ions within the polymer film to maintain charge neutrality.[5] Ion-exchange membranes (IEMs) are used in combination with electrochemical potential gradients to drive intercalation and deintercalation, typically through an ion-exchange mechanism, for the selective transport of certain ionic components between phases with different chemical compositions.[6,7] Such IEMs are critical to the operation of fuel cells,[8] electrolyzers,[9] redox flow batteries,[10] reverse electrodialyzers,[11] and microbial fuel cells.[12]

Electrochemical methods are particularly well suited to provide key information on the thermodynamics and kinetics of these ion-transfer processes. However, their use is restricted to matrices supported on electronically conductive substrates, as is the case for Li-ion battery cathodes[13−15] or conducting polymer films,[16,17] where reversible ion transfer is coupled with a redox reaction. The analysis of ion-transfer reactions in nonelectronically conductive solids, such as IEMs, is more difficult to study, given that ion transfer proceeds through an ion-exchange mechanism without a flow of electrons.[18,19] In

Received: June 2, 2020
Revised: July 16, 2020
Published: July 22, 2020

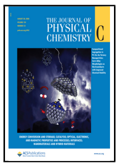

ACS Publications

https://dx.doi.org/10.1021/acs.jpcc.0c04976
J. Phys. Chem. C 2020, 124, 18346−18355

this sense, the interface between two immiscible electrolyte solutions (ITIES),[20,21] such as that formed between water and suitable hydrophobic organic solvents, offers an ideal platform to study the thermodynamics and kinetics of ion-transfer reactions involving nonelectronically conductive solids.

In the absence of redox-active species, polarization of the ITIES induces the movement of aqueous and organic electrolyte ions to, and across, the liquid|liquid interface.[22,23] Thus, a film of solid materials floating at the interface will experience a markedly different ionic environment and interfacial aqueous pH depending on the applied interfacial Galvani potential difference ($\Delta_{\mathrm{o}}^{\mathrm{w}}\phi/V$). In this article, we demonstrate that the interaction of charged or easily ionizable functional groups within the floating solid materials with the aqueous and organic electrolyte ions gives rise to capacitive currents associated with purely ionic reactions. Previous studies involving functionalization of the ITIES with nonconductive inorganic materials, such as zeolites[24−26] or silica,[27−31] were primarily motivated to develop sensor technology through charge- or size-selective ion transfer across the interface. Dryfe and co-workers have reported electrochemically driven ion exchange involving zeolites floating at the ITIES, but no in-depth thermodynamic or kinetic analysis was performed.[32−34]

Herein, we study the thermodynamics and kinetics of electrochemically reversible ion intercalation at a floating film of self-assembled zinc(II) 5,10,15,20-(tetra-4-carboxyphenyl)-porphyrin interfacial nanostructures (ZnPor-INs). The floating film effectively acts as an ion penetrable third phase separating the aqueous and organic phases. Cyclic voltammetry in the presence of the ZnPor-IN film was amenable to thermodynamic analysis using the Frumkin isotherm,[13−15] and kinetic analysis was performed using potential step chronoamperometry.[35] These purely ionic voltammetric and current transient responses were analogous to those commonly associated with reversible ion intercalation coupled with electron transfer, as described for Li-ion battery cathodes and conducting polymer films. The distinctive shape of the cyclic voltammograms (CVs) also indicated an electrochemically driven rearrangement of the porphyrin nanostructure at the liquid|liquid interface. These observations, connected with the presence of easily ionizable carboxyl groups within the ZnPor-IN film, were rationalized in terms of electrochemically driven binding of organic cations at anionic carboxyl ($-COO^-$) groups and ion exchange of organic cations at neutral carboxyl ($-COOH$) groups in which protons were displaced. This concept is schematically shown in Scheme 1 and S1 (Supporting Information).

■ RESULTS AND DISCUSSION

Electrochemistry of the Floating Film of ZnPor-INs at the ITIES. A film of ZnPor-INs was formed at the ITIES between a lithium citrate (Li_2HCit) buffered aqueous solution and an organic solution of bis(triphenylphosphoranylidene)-ammonium tetrakis(pentafluorophenyl)borate (R_2NTB) in TFT (see cell configuration in Scheme 2). The image of the film is shown in Figure S1. The molecular liquid|liquid boundary is located within the ZnPor-IN film, which is considered as a third phase separating the aqueous and organic solutions and a mixed-solvent layer.

Scheme 1. Electrochemically Driven Shifts in the Chemical Equilibria Involving Carboxyl Groups in the ZnPor-IN Film, Aqueous Protons H^+, and Organic Bulky Ammonium Cations R_2N^{+a}

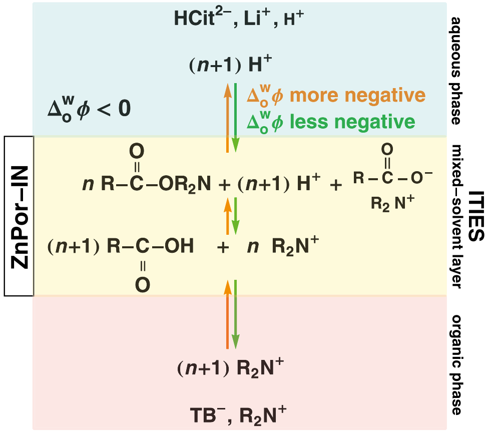

[a]The peak currents in the cyclic voltammograms (CVs) roughly correspond to negative $\Delta_{\mathrm{o}}^{\mathrm{w}}\phi$ such that the fractions of groups in $-COOH$ and $-COOR_2N$ forms are both large and similar to each other. As $\Delta_{\mathrm{o}}^{\mathrm{w}}\phi$ is scanned more negatively from the peak, R_2N^+ ions enter the film from the organic phase and the same amount of H^+ ions are transferred from the film to the aqueous phase. Two chemical equilibria are shifted: the acid dissociation of $-COOH$ and the exchange between bound H^+ and bound R_2N^+. For every $-COOH$ group involved in the acid dissociation, a larger number n is involved in the ion-exchange reaction. When $-COOH$ dissociates, the proton H^+ is displaced to the aqueous phase by a R_2N^+ ion that enters the film to compensate for the charge of $-COO^-$. Should $\Delta_{\mathrm{o}}^{\mathrm{w}}\phi$ be scanned to even more negative values, the R_2N^+ concentration in the film would be so that all carboxyl groups would be in the $-COOR_2N$ form and some $HCit^{2-}$ ions would enter the film to compensate for the charge of the R_2N^+ ions. Conversely, as $\Delta_{\mathrm{o}}^{\mathrm{w}}\phi$ is scanned from the peak to less negative values, H^+ ions enter the film from the aqueous phase and R_2N^+ ions are transferred from the film to the organic phase. Should $\Delta_{\mathrm{o}}^{\mathrm{w}}\phi$ be scanned to moderately positive values, Li^+ ions would enter the film to compensate for the charge of $-COO^-$. For full clarity, Scheme S1 in the Supporting Information provides another more detailed overview of the dynamics of the electrochemically driven reversible ion intercalation process.

Scheme 2. General Configuration of the Four-Electrode Cell Used for Electrochemical Measurements at the ZnPor-IN Functionalized Liquid|Liquid Interface[a]

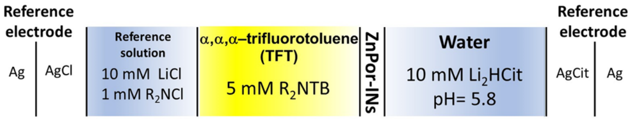

[a]The organic phase was 5 mM bis(triphenylphosphoranylidene)-ammonium tetrakis(pentafluorophenyl)borate (R_2NTB) in *α*,*α*,*α*-trifluorotoluene (TFT). The aqueous phase was lithium citrate (Li_2HCit) at pH 5.8 (unless otherwise stated). The ZnPor-IN films were prepared from solutions of ZnPor at concentrations in the range of 10−100 μM in contact with the TFT for 30 min, as described in the Experimental Section of the Supporting Information.

Cyclic voltammograms (CVs) were obtained with a four-electrode electrochemical cell, using the configuration outlined in Scheme 2, both in the absence and presence of the floating ZnPor-IN film at a scan rate of 1 $mV \cdot s^{-1}$. The interfacial concentration Γ_{ZnPor} of ZnPor in the film was determined spectroscopically (Figure S2), as described in the Experimental Section (see Supporting Information) prior to all electrochemical measurements. The control CV in the absence of the

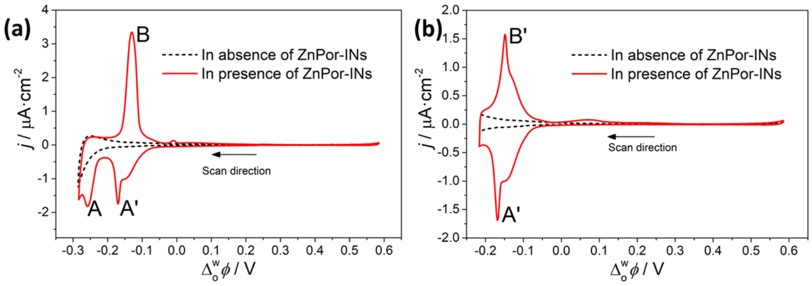

Figure 1. Cyclic voltammetry in the absence (dashed lines) and presence (solid lines) of the ZnPor-IN film at the ITIES. The electrochemical configuration of the four-electrode electrochemical cell was as described in Scheme 2. The influence of systematically varying the lower vertex potential on the CVs was investigated by switching the potential on the negative scan at (a) −0.285 V and (b) −0.215 V. The scan rate was 1 mV·s^{-1} and the start potential was 0.250 V. The interfacial concentration of ZnPor was Γ_{ZnPor} = 0.88 nmol·cm^{-2}.

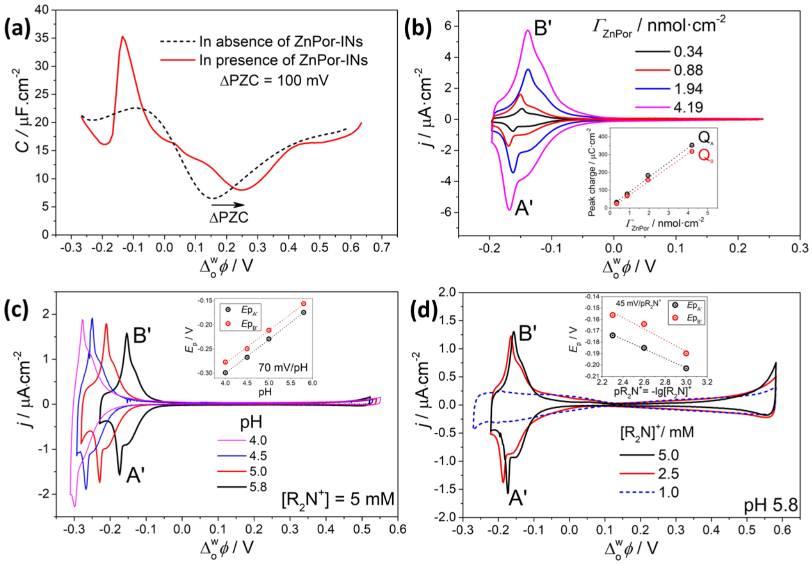

Figure 2. (a) Monitoring the potential of zero charge (PZC) by obtaining differential capacitance curves in the absence (dashed line) and presence (solid line) of the ZnPor-IN film. The capacitance was calculated from impedance measurements every 5 mV at 80 Hz assuming an *RC* circuit where *R* represents the solution resistance and *C* the double-layer capacitance. Γ_{ZnPor} was determined spectroscopically as 0.34 nmol·cm^{-2}. (b) Cyclic voltammetry in the presence of ZnPor-IN films of increasing Γ_{ZnPor}. The scan rate used was 1 mV·s^{-1}. Inset: the dependence of the peak charge *Q* on Γ_{ZnPor}. The effect of varying (c) the pH and (d) the R_2NTB concentration on the electrochemical response was investigated in the presence of the ZnPor-IN film. The scan rate used was 5 mV·s^{-1} and Γ_{ZnPor} was 0.34 nmol·cm^{-2}. Insets in (c) and (d): the relationships between the peak potential E_p and pH or pR_2N^+ (= −lg $[R_2N^+]$), respectively. For clarity, a zoomed-in version of the CV obtained with $[R_2N^+]$ = 1 mM (dashed blue line) in (d) is shown in Figure S6.

film was essentially featureless (dashed line, Figure 1a). The only signal observed upon varying the applied interfacial Galvani potential difference $\Delta_o^w\phi$ was due to the aqueous background electrolyte citrate anions being transferred to the organic phase at the negative extreme of the polarizable potential window (PPW). By contrast, in the presence of the ZnPor-IN film, several electrochemical signals were observed at negative potentials (solid line, Figure 1a). The absence of redox-active species in either phase means that the electrochemical signals in the presence of the ZnPor-IN film were purely ionic in nature.

The relationship between the two electrochemical signals on the negative scan with negative currents (labeled A and A′ in Figure 1a) and the signal on the positive scan with a positive current (labeled B in Figure 1a) was investigated by systematically varying the lower vertex potential (Figure 1b). Switching the potential on the negative scan immediately after the appearance of peak A′ led to a major reduction in the magnitude of the electrochemical signal on the positive scan. Labeled B′, this smaller peak was of a near-identical shape and magnitude to A′ (Figure 1b). Therefore, the electrochemical process giving rise to peak A′ was the reverse of that giving rise to peak B′. Indeed, the ratio of the magnitude of the charge for each peak was $Q_{A'}/Q_{B'} \approx 1$ for CVs obtained at scan rates ranging from 5 to 50 mV·s^{-1} and close to 0.9 at all Γ_{ZnPor} at 1 mV·s^{-1} (Figure S3 and Tables S1 and S2). Furthermore, as peaks A and A′ were related to peak B, both A and A′ were associated with the same species.

The peak-to-peak separation between peaks A′ and B′ was 5.9 mV at a scan rate of 1 mV·s^{-1}. Additionally, the peak current i_p for peaks A′ and B′ varied linearly with the scan rate (Figure S3). Thus, the kinetics of these electrochemical signals were controlled by surface processes in the presence of the ZnPor-IN film. In the electrochemical configuration described in Scheme 2, no ionic species were present that were capable of undergoing ion transfer across the ITIES within the PPW. Therefore, the electrochemical signals observed in the presence of the ZnPor-IN film were due to a diffusion-less process, that is, adsorption and capacitive phenomena, and not faradic ion transfer.

Scheme 3. ZnPor-IN-Functionalized Liquid|Liquid Interface Behaves as a Capacitor[a]

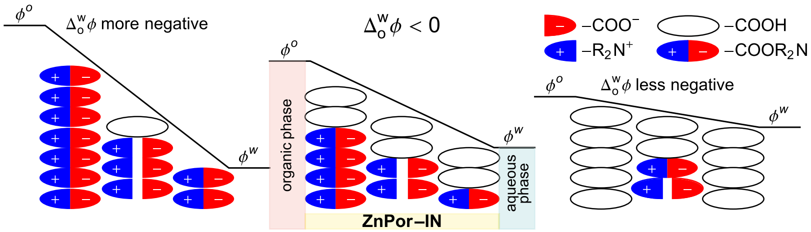

[a]Carboxyl groups in the −COOH form are taken as a reference corresponding to the absence of charges in the capacitor plates. When $\Delta_o^w\phi$ is scanned progressively negative, the R_2N^+ ions are pushed into the film, a few −COOH groups are forced to dissociate, and many more transform into $-COOR_2N$. The released H^+ ions are pulled into the aqueous phase.

The self-assembly of the floating ZnPor-IN film at the ITIES was optimal at pH 5.8.[36] As this pH matched the pK_a of the ZnPor carboxyl groups, statistically, 50% of them were deprotonated and charged in the bulk aqueous solution. Differential capacitance measurements are a macroscopic view of the charge distribution of the back-to-back diffusion layers or mixed-solvent region.[23,37−41] The capacitance minimum appears at the potential of zero charge (PZC). Figure 2a shows differential capacitance measurements obtained in the presence and absence of the ZnPor-IN film. Capacitance values were calculated from the imaginary part of the impedance at a frequency of 80 Hz. This frequency was selected to suppress faradic contributions due to ion transfer within the PPW. This effect is demonstrated in Figure S4a where the faradic current due to the ion transfer of tetraethylammonium cations across a bare water|TFT interface was entirely filtered out at 80 Hz. A shift in the PZC of +100 mV was observed in the presence of the ZnPor-IN film (Figure 2a). This shift confirms a negative excess charge at the interface due to the presence of deprotonated carboxyl groups at this pH.[36] The peak at −0.15 V was seen at all frequencies across a range from 5 to 80 Hz (Figure S4b), further confirming that these electrochemical signals in the presence of the ZnPor-IN film were associated with adsorption and capacitive processes.

The electrochemical signals in Figure 1 appear at negative $\Delta_o^w\phi$, suggesting the binding of R_2N^+ cations to the carboxyl groups of the ZnPor. These groups may exist in three states: $-COO^-$, −COOH, and $-COOR_2N$. Their concentrations c_{COO^-}, c_{COOH}, and c_{COOR_2N} can vary with the bulk aqueous pH, the applied $\Delta_o^w\phi$, as well as with the Li_2HCit and R_2NTB concentrations. On the contrary, the total concentration

$$c_{T,COO} = c_{COO^-} + c_{COOH} + c_{COOR_2N} \tag{1}$$

is a constant related to Γ_{ZnPor}. To corroborate the relation with $c_{T,COO}$, Γ_{ZnPor} was systematically varied by increasing the bulk aqueous ZnPor concentration during the ZnPor-IN film self-assembly. A linear increase in the charge for each peak, $Q_{A'}$ and $Q_{B'}$, was observed (Figure 2b). This linear increase was obtained despite Γ_{ZnPor} far exceeding that expected for an interfacial monolayer of ZnPor (estimated as 0.095 nmol·cm^{-2}, see Figure S5). Thus, the electrochemical signals were due to processes involving carboxyl groups within the ZnPor-IN film, and not only at surface sites facing the aqueous and organic electrolytes.

To probe the effects of the bulk aqueous pH and R_2N^+ concentration, both were varied independently (Figure 2c,d). As we described previously,[36] ZnPor-INs were stabilized by cooperative hydrogen bonding. Thus, pH conditions more alkaline than the carboxyl groups' pK_a of 5.8 were ruled out as the ZnPor-IN film would destabilize and dissolve. The peak potentials for peaks A′ ($E_{pA'}$) and B′ ($E_{pB'}$) were found to depend on both the pH and pR_2N^+ (where pR_2N^+ = −lg[R_2N^+]), confirming their role in the electrochemical processes occurring at the ZnPor-IN-functionalized ITIES. The uniform shifts of −70 mV/pH and +45 mV/pR_2N^+ were observed for both $E_{pA'}$ and $E_{pB'}$ (insets, Figure 2c,d). The magnitude of peaks A′ and B′ decreased drastically at the lowest R_2N^+ concentration investigated ([R_2N^+] = 1 mM), as shown in Figures 2d and S6.

The influence of the nature of the aqueous anion on the electrochemical response was also investigated. Citrate anions are sensitive to pH, with pK_a's at 3.13, 4.76, and 6.40, respectively.[42] Thus, as the pH at the ITIES varies as a function of applied $\Delta_o^w\phi$, a pH-insensitive anion was chosen for comparison by replacing Li_2HCit with LiCl. As shown in Figure S7, the nature of the anion had a minimal effect on the electrochemical response. A near-identical CV shape was observed, and the trend in the shifts of $E_{pA'}$ and $E_{pB'}$ with pH was replicated.

Peaks A′ and B′ in the CVs in Figures 1 and 2b−d are formed by the superposition of a narrow peak and a broad peak. Narrow "adsorption" peaks in CVs are considered to indicate positive cooperativity, that is, every adsorption event is facilitated by the occurrence of a previous adsorption event. In this regard, for fundamental thermodynamic reasons, the CVs can be described using the Frumkin isotherm.[15] For peak B′, we attribute the broad shoulders to the binding of R_2N^+ at $-COO^-$ groups and ion exchange of R_2N^+ with −COOH groups (in which protons are displaced) near the o|IN interface as R_2N^+ flows from the organic phase into the ZnPor-IN film. The sharp peak of B′ is attributed to the binding and ion exchange of R_2N^+ at $-COO^-$ and −COOH groups, respectively, deeper inside the ZnPor-IN film. The second electrochemical signal on the negative scan, peak A, is attributed to a second binding and ion-exchange event inside the ZnPor-IN film requiring more electrochemical driving force (see Figure 1a). As detailed in the following section, all peaks are capacitive in nature and resemble adsorption due to a saturation limit to the concentration of $-COOR_2N$ species that form by binding and ion exchange as $\Delta_o^w\phi$ is scanned negatively.

Modeling of Electrochemically Driven Reversible Ion Intercalation in the Presence of the ZnPor-IN film. The modeling aims to clarify: (i) the capacitive nature of the electrochemical signals at negative $\Delta_o^w\phi$ in the presence of the ZnPor-IN film, (ii) the trends in the shifts of the peak potentials as a function of the bulk aqueous pH and R_2N^+ concentration, and (iii) the characteristic CV shapes indicative

https://dx.doi.org/10.1021/acs.jpcc.0c04976
J. Phys. Chem. C 2020, 124, 18346−18355

of positive cooperativity. For the electrolyte concentrations used in the electrochemical experiments, the film thickness, $L^{\mathrm{IN}} \approx 100$ nm,[36] is much larger than the aqueous and organic Debye lengths and the molecular liquid|liquid boundary is located within the ZnPor-IN film. Thus, the film is considered as an intermediate phase (IN) separating the aqueous (w) and organic (o) solutions. From the point of view of ion solvation, it is a mixed-solvent layer, disliked by both aqueous ions and organic ions.

Within the PPW, no ions can transfer across the ITIES and the ZnPor-IN film behaves as a capacitor (Scheme 3). When $\Delta_{\mathrm{o}}^{\mathrm{w}}\phi$ is scanned progressively more negative, the R_2N^+ ions are "pushed" into the film but cannot transfer to the aqueous phase. Then, a few −COOH groups are forced to dissociate, and many more transform into $-COOR_2N$. In both cases, the released H^+ ions are "pulled" into the aqueous phase. The charge of the anionic carboxyl groups $-COO^-$ is mostly compensated for by R_2N^+, which are the majority ions in the film; $HCit^{2-}$ and Li^+ are present only when $\Delta_{\mathrm{o}}^{\mathrm{w}}\phi$ is very different to that around the peaks in Figure 2b. To understand the behavior of the film as a capacitor, carboxyl groups in the −COOH form are taken as a reference corresponding to the absence of charges in the capacitor "plates". The positive plate accumulates charge in the form of free R_2N^+ and bound R_2N^+, that is, the charge q° in this positive plate is basically proportional to $c_{\mathrm{COOR_2N}} + c_{\mathrm{R_2N}}^{\mathrm{IN}}$. The negative plate has a charge $q^{\mathrm{w}} < 0$, which is a measure of the reduction in the amount of −COOH groups and hence proportional to $c_{\mathrm{T,COO}} - c_{\mathrm{COOH}}$. As $\Delta_{\mathrm{o}}^{\mathrm{w}}\phi$ is made more negative, $q^{\circ} = -q^{\mathrm{w}} > 0$ increases but remains of the order of $c_{\mathrm{T,COO}}$. The unfavorable solvation in this mixed-solvent layer keeps the free-ion concentrations $c_{\mathrm{R_2N}}^{\mathrm{IN}}$ and $c_{\mathrm{HCit}}^{\mathrm{IN}}$ to relatively small values, even for the most negative $\Delta_{\mathrm{o}}^{\mathrm{w}}\phi$.

The concentrations of the ionic species R_2N^+, TB^-, $HCit^{2-}$, H^+, and Li^+ in the film (phase IN) must satisfy the local electroneutrality condition

$$c_{\mathrm{COO^-}} + 2c_{\mathrm{HCit}}^{\mathrm{IN}} + c_{\mathrm{TB}}^{\mathrm{IN}} = c_{\mathrm{R_2N}}^{\mathrm{IN}} + c_{\mathrm{Li}}^{\mathrm{IN}} + c_{\mathrm{H}}^{\mathrm{IN}} \tag{2}$$

The local electroneutrality condition can also be presented as $q^{\circ} + q^{\mathrm{w}} = 0$, where

$$q^{\circ} = FL^{\mathrm{IN}}(c_{\mathrm{COOR_2N}} + c_{\mathrm{R_2N}}^{\mathrm{IN}} - c_{\mathrm{TB}}^{\mathrm{IN}}) \tag{3}$$

$$-q^{\mathrm{w}} = FL^{\mathrm{IN}}(c_{\mathrm{T,COO}} - c_{\mathrm{COOH}} + 2c_{\mathrm{HCit}}^{\mathrm{IN}} - c_{\mathrm{H}}^{\mathrm{IN}} - c_{\mathrm{Li}}^{\mathrm{IN}}) \tag{4}$$

are the charge densities in the capacitor and F is Faraday's constant. In the potential range $-0.25\ \mathrm{V} < \Delta_{\mathrm{o}}^{\mathrm{w}}\phi < -0.05\ \mathrm{V}$, the concentrations of R_2N^+, $HCit^{2-}$, and $-COO^-$, $c_{\mathrm{R_2N}}^{\mathrm{IN}}$, $c_{\mathrm{HCit}}^{\mathrm{IN}}$, and $c_{\mathrm{COO^-}}$, are the dominant terms in eq 2. For $\Delta_{\mathrm{o}}^{\mathrm{w}}\phi > -0.05$ V, the concentrations $c_{\mathrm{Li}}^{\mathrm{IN}}$ and $c_{\mathrm{TB}}^{\mathrm{IN}}$ of the Li^+ and TB^- species may become significant. Although some species make a negligible contribution in eq 2, we keep them all for the sake of generality. The electrical double layers at the o|IN and IN|w interfaces extend over a fraction of the film thickness L^{IN}, and local electroneutrality does not hold there. However, the contributions of the associated interfacial capacitances are small compared to other effects described below and, therefore, can be neglected.

The concentrations of the ionic species in phase IN are different from those in their respective phases. In absolute value, the Gibbs energy of transfer of the organic ions from phase o to phase IN is intermediate to that from phase o to phase w. Similarly, in absolute value, the Gibbs energy of transfer of the aqueous ions from phase w to phase IN is intermediate to that from phase w to phase o. Therefore, the ions have no chemical preference to enter phase IN, and their chemical partition coefficients into this phase are significantly lower than unity, $P_i \ll 1$. The applied potential $\Delta_{\mathrm{o}}^{\mathrm{w}}\phi$ also affects the distribution of the ions. The potential ϕ^{IN} is usually intermediate between phases w and o so that $\Delta_{\mathrm{IN}}^{\mathrm{w}}\phi = \phi^{\mathrm{w}} - \phi^{\mathrm{IN}}$, $\Delta_{\mathrm{o}}^{\mathrm{IN}}\phi = \phi^{\mathrm{IN}} - \phi^{\mathrm{o}}$, and

$$\Delta_{\mathrm{o}}^{\mathrm{w}}\phi = {}_{\mathrm{IN}}^{\mathrm{w}}\phi + {}_{\mathrm{o}}^{\mathrm{IN}}\phi \tag{5}$$

have the same sign. The distribution equilibrium of, for example, the organic cation R_2N^+ between phases o and IN requires $c_{\mathrm{R_2N}}^{\mathrm{IN}} = c^{\mathrm{o,b}}\ P_{\mathrm{R_2N}}e^{-f\Delta_{\mathrm{o}}^{\mathrm{IN}}\phi}$, where $c^{\mathrm{o,b}} = [R_2N^+]$ is its concentration in the bulk organic phase. Similar equations can be formulated for the other species, as described in detail in the Supporting Information.

The evaluation of the concentrations $c_{\mathrm{COO^-}}$, c_{COOH}, and $c_{\mathrm{COOR_2N}}$ in eqs 2−4 requires the simultaneous consideration of the ionic distribution equilibria and the chemical equilibria. Since $c_{\mathrm{H}}^{\mathrm{IN}} = c_{\mathrm{H}}^{\mathrm{w,b}}P_{\mathrm{H}}e^{f\Delta_{\mathrm{IN}}^{\mathrm{w}}\phi}$, both the negative $\Delta_{\mathrm{o}}^{\mathrm{w}}\phi$ and the mixed-solvent nature of phase IN contribute to increasing the interfacial pH with respect to the bulk aqueous pH, $\mathrm{pH}^{\mathrm{IN}} - \mathrm{pH} = -\lg(c_{\mathrm{H}}^{\mathrm{IN}}/c_{\mathrm{H}}^{\mathrm{w,b}}) > 0$. Yet, if the latter is equal to or lower than the $\mathrm{p}K_{\mathrm{a}} = 5.8$ of the carboxyl groups, some of these groups can be protonated according to the equilibrium

$$K_{\mathrm{a}}^{\mathrm{IN}}c^{\circ} = \frac{c_{\mathrm{H}}^{\mathrm{IN}}c_{\mathrm{COO^-}}}{c_{\mathrm{COOH}}} \tag{6}$$

where $c^{\circ} = 1$ M and $K_{\mathrm{a}}^{\mathrm{IN}} = K_{\mathrm{a}}P_{\mathrm{H}}$; see eq S32 in the Supporting Information. The abundant R_2N^+ cations in phase IN can displace the bound protons and form $-COOR_2N$ groups. The equilibrium of the ion-exchange reaction

$$\begin{aligned} &-\mathrm{COOH(IN)} + \mathrm{R_2N^+(IN)} \\ &\quad \rightleftarrows -\mathrm{COOR_2N(IN)} + \mathrm{H^+(IN)} \end{aligned} \tag{7}$$

requires

$$K_{\mathrm{IE}}^{\mathrm{o,IN}} = \frac{c_{\mathrm{H}}^{\mathrm{IN}}c_{\mathrm{COOR_2N}}}{c_{\mathrm{R_2N}}^{\mathrm{IN}}c_{\mathrm{COOH}}} \tag{8}$$

where $K_{\mathrm{IE}}^{\mathrm{o,IN}}$ is the equilibrium constant. From eqs 1, 6, and 8, the fraction of charged carboxyl groups is

$$\frac{c_{\mathrm{COO^-}}}{c_{\mathrm{T,COO}}} = \frac{K_{\mathrm{a}}^{\mathrm{IN}}c^{\circ}}{K_{\mathrm{a}}^{\mathrm{IN}}c^{\circ} + c_{\mathrm{H}}^{\mathrm{IN}} + K_{\mathrm{IE}}^{\mathrm{o,IN}}c_{\mathrm{R_2N}}^{\mathrm{IN}}} \tag{9}$$

Substituting $c_{\mathrm{COO^-}}$ from eq 9 into eq 2, and using the conditions of distribution equilibria of the ionic species, the potential drop $\Delta_{\mathrm{IN}}^{\mathrm{w}}\phi$ can be determined, see eq S17 in the Supporting Information. Hence, the ionic concentrations and q° are known as functions of $\Delta_{\mathrm{o}}^{\mathrm{w}}\phi$, as well as the differential capacitance of the ZnPor-IN film

$$C = -\mathrm{d}q^{\circ}/\mathrm{d}\Delta_{\mathrm{o}}^{\mathrm{w}}\phi \tag{10}$$

The applied potential $\Delta_{\mathrm{o}}^{\mathrm{w}}\phi$ affects the distribution of the ions and hence also the ion-exchange equilibrium. Thus, eq 8 can be transformed to

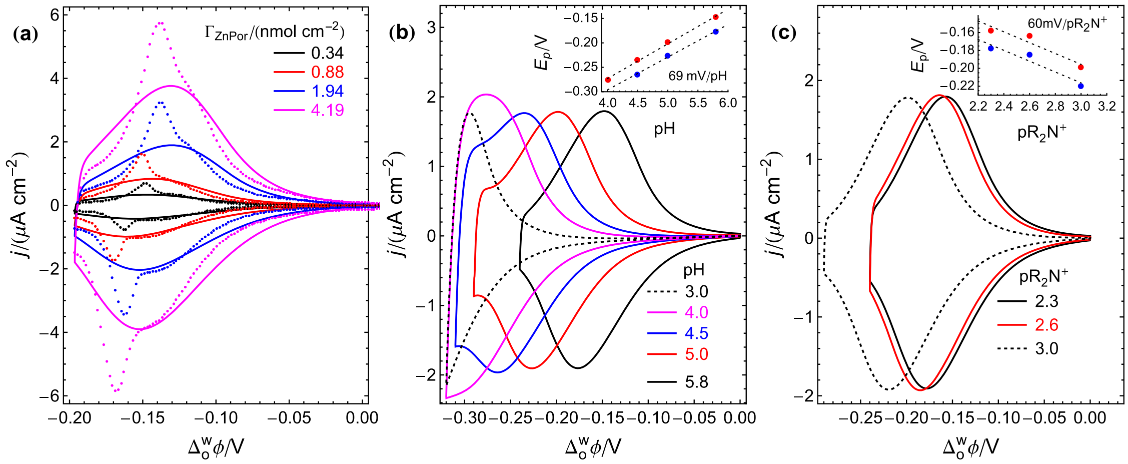

Figure 3. CVs generated using the theoretical model qualitatively capture the main features of the experimental CVs at the ITIES in the presence of a ZnPor-IN film. (a) Comparison of the simulated (lines) and experimental CVs (symbols) at 1 mV·s^{-1} for the electrochemical cell described in Scheme 2 (with 5 mM R_2NTB, 10 mM Li_2HCit, a bulk aqueous pH = 5.8, and varying Γ_{ZnPor}). In particular, the peak separation and the total charge under the peaks are well reproduced, though the shape of the peaks is not. The simulated CVs accurately describe the experimentally observed values of peak potentials and their linear shift with (b) the pH and (c) the R_2NTB concentration at 5 mV·s^{-1} and Γ_{ZnPor} = 0.34 nmol·cm^{-2}. The parameter values for the simulations in panels (a)−(c) are shown in Tables S3 and S4.

$$\frac{c_{COOR_2N}}{c_{COOH}} = K_{IE}^{o,IN}\frac{c^{o,b}P_{R_2N}}{c_H^{w,b}P_H}e^{-f\Delta_o^w\phi} \tag{11}$$

As $\Delta_o^w\phi$ is scanned progressively negative, $q^o = -q^w > 0$ increases. Across the IN|w interface, $GCit^{2-}$ ions may flow from phase w to phase IN (if $\Delta_o^w\phi$ is sufficiently negative); the flow of Li^+ and H^+ ions from phase IN to phase w is usually negligible. Across the o|IN interface, R_2N^+ ions flow into phase IN; the flow of TB^- ions from phase IN to phase o is usually much smaller. The increase in $c_{R_2N}^{IN} = c^{o,b}P_{R_2N}e^{-f\Delta_o^{IN}\phi}$ shifts the ion-exchange equilibria toward the formation of $-COOR_2N$, at the expense of reducing c_{COO^-} and c_{COOH}. The increase in c_{COOR_2N} gives rise to an adsorption peak in the CV because there is a saturation limit, $c_{COOR_2N} \leq c_{T,COO}$. By convention, a positive charge flow from o to w gives rise to a peak in the CV of negative current.[20,21] Similarly, as $\Delta_o^w\phi$ is made more positive, $q^w = -q^o > 0$ increases. Across the o|IN interface, R_2N^+ ions flow toward phase o. Across the IN|w interface, $HCit^{2-}$ ions flow toward phase w. During such a potential scan, c_{COOR_2N} decreases as c_{COO^-} and c_{COOH} increase. The increase in c_{COO^-} gives rise to an adsorption peak with a positive current in the CV (negative charge flow from o to w).

The CVs can be simulated using an equivalent electrical circuit consisting of the solution resistance R_{sol} in series with the parallel combination of the film capacitance C and the charge transfer resistance R_{ct} (see eqs S19 and S20, Supporting Information). This simple theoretical model qualitatively captures the main features of the experimental CVs, such as the total charge under the peaks, the peak separation, and their variation with the bulk aqueous pH and the organic electrolyte concentration (see Figure 3 and Tables S3 and S4). However, this model does not accurately reproduce the shape of the peaks. The experimental peaks are the superposition of a narrow peak and a broad peak, the former occurring at a more negative $\Delta_o^w\phi$ and having a smaller area (and hence charge) under the peak. Even the broad peak is narrower than predicted by this model.

The narrow adsorption peaks in the CVs are considered an indication of positive cooperativity. Herein, we propose that once the initial bulky R_2N^+ cations flow across the o|IN interface as $\Delta_o^w\phi$ is scanned negatively, they "open" space in the nanostructure due to structural rearrangements of the porphyrins allowing the later R_2N^+ species to penetrate the ZnPor-IN film much more easily. Thus, this conformational change of ZnPor-INs is the physical reason behind the negative g interaction parameters discussed vide infra, which is characteristic of positively cooperative adsorption. Furthermore, the characteristic shape of the purely capacitive CVs due to structural rearrangements of the porphyrins at the electrified liquid|liquid interface precisely resembles those of systems involving phase transitions at electrified solid|liquid interfaces, for example, electrochemically driven structural changes of a copper adlayer on a Au(111) electrode surface.[43]

The cooperative binding of R_2N^+ ions can be described using the Frumkin isotherm, described in detail in the Supporting Information. As mentioned above, the peaks in the experimental CVs are formed by the superposition of a narrow peak and a broad peak. Accordingly, we have simulated the CV by adding the theoretical curves calculated with two sets of carboxyl groups, described by eq S24 in the Supporting Information. The set responsible for the narrow peak has a more negative Frumkin parameter g_{narrow} and a smaller constant $K_{IE,narrow}^{o,IN}$ so that the peak appears at a more negative $\Delta_o^w\phi$, compared to the less negative g_{broad} and larger $K_{IE,broad}^{o,IN}$ corresponding to the set responsible for the broad peak. The electrical parameters R_{sol} and R_{ct} in eq S20, Supporting Information, are common to both sets (Table S5). At 298 K, $g_{narrow} = -3.5$ and $g_{broad} = -0.7$ correspond to attractive interaction energies $z_c\varepsilon_{narrow} = g_{narrow}RT = -8.67$ kJ·mol^{-1} and $g_{broad}RT = -1.73$ kJ·mol^{-1}. These g values seem reasonable on the basis of the excellent agreement (Figures 4 and S7) between the simulated and the experimental CVs, given the complexity of the system under consideration. Moreover, a value $g = -4.2$ is observed for a Li^+ intercalation process, a system with very similar underlying thermodynamics.[13]

Kinetics of Electrochemically Driven Reversible Ion Intercalation in the Presence of the ZnPor-IN film. As

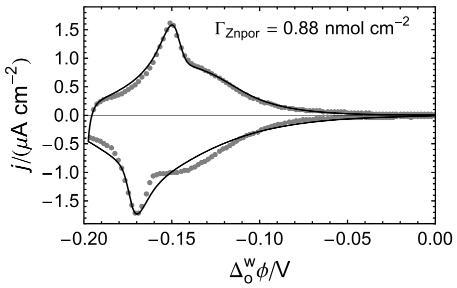

Figure 4. Consideration of two types of binding sites, described by eq S24in the Supporting Information, with g_{narrow} = −3.5 and g_{broad} = −0.7, predicts simulated CVs (lines) at 1 mV·s^{-1} and Γ_{ZnPor} = 0.88 nmol·cm^{-2} that resemble more closely the experimental observations (symbols). Comparisons are provided for CVs obtained with Γ_{ZnPor} values of 0.34, 1.94, and 4.19 nmol·cm^{-2} in Figure S8. The parameter values (Table S5) have been chosen on the basis of a qualitative agreement and not using a fitting algorithm.

$\Delta_o^w\phi$ is scanned progressively negative, ion intercalation of R_2N^+ from the organic phase into the ZnPor-IN film proceeds by binding and ion exchange, with $c_{COOR_2N}^{IN}$ increasing. The aim of this section is to investigate the kinetics of this process by potential step chronoamperometry. A particular focus is placed on the influence of both $\Delta_o^w\phi$ and Γ_{ZnPor} on the rates of the charge transfer processes. Current transients were obtained by maintaining a constant initial potential $\Delta_o^w\phi_{initial}$ for $t_{initial}$ = 30 s and varying the final potential $\Delta_o^w\phi_{final}$ in 50 mV increments across the region where the electrochemical signals were observed (−0.05 V > $\Delta_o^w\phi$ > −0.30 V), see Figures S9 and 5a,b. The value $\Delta_o^w\phi_{initial}$ = +0.25 V was chosen because no discernible electrochemical processes were occurring at that $\Delta_o^w\phi$, besides capacitive charging of the back-to-back double layers at the ITIES. Once more, four electrochemical cells with increasing Γ_{ZnPor} (0.34, 0.88, 1.94, and 4.19 nmol·cm^{-2}) were investigated.

Depending on $\Delta_o^w\phi_{final}$ and Γ_{ZnPor}, the current transients presented a decay component, commonly associated with an adsorption process, and multiple rising components with current maxima, commonly associated with nucleation and growth processes. In this regard, these current transients obtained by potential step chronoamperometry are highly reminiscent of those generated using the same technique to study the kinetics of structural changes during the electrochemical switching of electronically conducting polymer films, such as polypyrrole, between their reduced (insulating) and oxidized (electronically conducting) states.[35] The kinetics of processes in conducting polymers that lead to a current maximum after a potential step are described by the electrochemically stimulated conformational relaxation (ESCR) model.[44,45] In common with conducting polymer films, electrochemically driven processes (binding and ion exchange) in the ZnPor-IN film occur throughout a three-dimensional volume, with ion intercalation steps linked to morphological changes in the film structures.

A key question is: how do we define the meaning of "nucleation" in the context of the ZnPor-IN film at the ITIES? Herein, we propose that the presence of nucleation transients was associated with domains within the nanostructures where, due to structural rearrangements of the porphyrins, the binding and ion exchange of R_2N^+ at $-COO^-$ and $-COOH$ groups, respectively, took place faster. Also, the energetically less demanding binding and ion exchange of further R_2N^+ species after these structural rearrangements of the porphyrins is the physical reason underlying the electrochemical observation of positively cooperative behavior discussed earlier.

Prior to kinetic analysis, the initial 50 ms (the value obtained from impedance measurements for the *RC* constant of the cell)

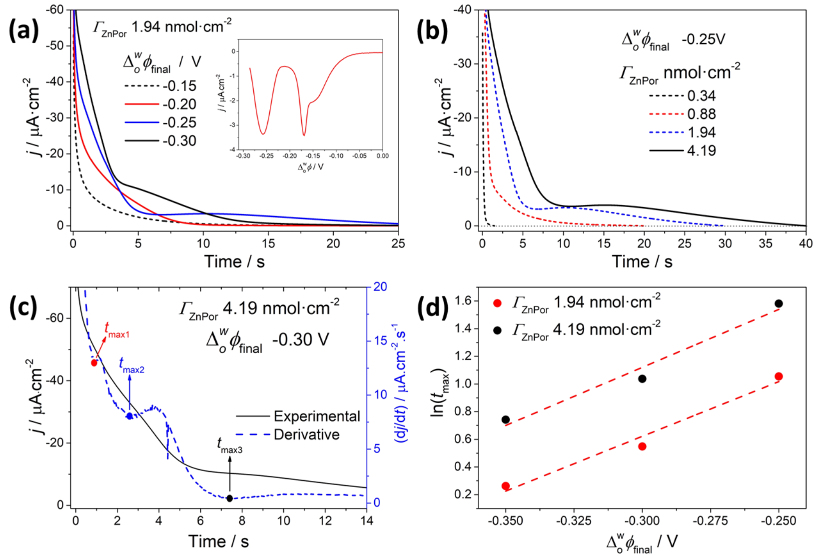

Figure 5. Kinetics of electrochemically driven reversible ion intercalation by potential step chronoamperometry in the presence of the ZnPor-IN film. (a) Current transients probing the influence of $\Delta_o^w\phi_{final}$ were obtained by varying $\Delta_o^w\phi_{final}$ in 50 mV increments at a constant Γ_{ZnPor} of 1.94 nmol·cm^{-2} and $\Delta_o^w\phi_{initial}$ of +0.25 V for 30 s ($t_{initial}$). (b) Current transients probing the influence of Γ_{ZnPor} were obtained by increasing Γ_{ZnPor} from 0.34 to 4.19 nmol·cm^{-2} while maintaining a constant $\Delta_o^w\phi_{initial}$ of +0.25 V for 30 s and $\Delta_o^w\phi_{final}$ of −0.25 V. (c) Deconvolution of the t_{max} values of the nucleation components from an experimental current transient (solid black line, obtained with a Γ_{ZnPor} of 4.19 nmol·cm^{-2}, $\Delta_o^w\phi_{initial}$ of +0.25 V for 30 s, and $\Delta_o^w\phi_{final}$ of −0.30 V) by obtaining the derivative (dashed blue line). (d) Plot of ln(t_{max}/s) versus $\Delta_o^w\phi_{final}$ for current transients obtained with a $\Delta_o^w\phi_{initial}$ of +0.25 V for 30 s and Γ_{ZnPor} of either 1.94 nmol·cm^{-2} (red circles) or 4.19 nmol·cm^{-2} (black circles). The t_{max} data is obtained for the second nucleation component, designated as t_{max2} in Table S6.

were neglected and the residual current was subtracted such that $j = 0$ A·cm^{-2} at $t = 40$ s. For all Γ_{ZnPor} values, the transients obtained using −0.05, −0.10, and −0.15 V as $\Delta_{\text{o}}^{\text{w}}\phi_{\text{final}}$ (and +0.25 V as $\Delta_{\text{o}}^{\text{w}}\phi_{\text{initial}}$) did not show any significant nucleation component (Figure S9). Thus, the analysis was focused on the transients obtained using −0.25, −0.30, and −0.35 V as $\Delta_{\text{o}}^{\text{w}}\phi_{\text{final}}$, where the nucleation features were observed (Figure 5a,b). In many cases, more than one nucleation component was observed experimentally, up to a maximum of three. The latter may be associated with binding and ion exchange at inner carboxyl sites. Therefore, the nucleation components were deconvoluted from the total current signal by plotting the derivative of the total current. From the derivative, the time t_{max} of the peak current maximum for each nucleation component within each transient was easily identified, see Figure 5c. A summary of these t_{max} values as a function of Γ_{ZnPor} and $\Delta_{\text{o}}^{\text{w}}\phi_{\text{final}}$ is presented in Table S6. Using these t_{max} values as a clear guide to the number of nucleation components present, the total fitted current for any transient may be obtained as a summation of the adsorption and nucleation components using exponential decay and Gaussian-type functions, respectively (Figure S10).

An increase in nucleation kinetics will be reflected in a shorter time required to reach t_{max} for each nucleation component. For all values of Γ_{ZnPor} and $\Delta_{\text{o}}^{\text{w}}\phi$, the shifts of t_{max} followed consistent trends. At a constant Γ_{ZnPor} and $\Delta_{\text{o}}^{\text{w}}\phi_{\text{initial}}$, an increase in nucleation kinetics (decreasing t_{max}) was seen as $\Delta_{\text{o}}^{\text{w}}\phi_{\text{final}}$ was set to more negative values (Figure 5a and Table S6). In other words, conformational relaxation to the more open nanostructure is faster as more energy is applied to drive R_2N^+ species into the ZnPor-IN film, leading to the creation of more nuclei. Conversely, at a constant $\Delta_{\text{o}}^{\text{w}}\phi_{\text{initial}}$ of +0.25 V and $\Delta_{\text{o}}^{\text{w}}\phi_{\text{final}}$ of −0.25 V, a decrease in nucleation kinetics (increasing t_{max}) was seen as Γ_{ZnPor} increased (Figure 5b and Table S6). The latter indicates that more energy is required to achieve conformational relaxation as Γ_{ZnPor} increases. A prediction of the ESCR model is that a linear relationship exists between $\ln(t_{\text{max}}/\text{s})$ and the energy required to relax and swell the conducting polymer film by oxidation, that is, the anodic overpotential.[46] In line with this prediction, the plots of $\ln(t_{\text{max}}/\text{s})$ versus $\Delta_{\text{o}}^{\text{w}}\phi_{\text{final}}$ for one of the nucleation sites (designated t_{max2}) are linear and exhibit the same slope for the higher Γ_{ZnPor} studied, 1.94 and 4.19 nmol·cm^{-2} (Figure 5d). The latter identical slopes indicate that the rate of increase in nucleation kinetics (decreasing t_{max}) as $\Delta_{\text{o}}^{\text{w}}\phi_{\text{final}}$ shifts negatively is independent of Γ_{ZnPor} in the range studied, highlighting that the liquid−liquid interface buried within the nanostructure has a finite thickness.

Finally, the effect of the initial "compaction" of the ZnPor-IN film on the kinetics was evaluated using two different experimental approaches. As R_2N^+ are bulky organic cations, far larger than the protons they displace from −COOH groups, it can be reasonably assumed that the volume of the ZnPor-IN film swells at negative $\Delta_{\text{o}}^{\text{w}}\phi$ values, reducing the compaction of the films. First, Γ_{ZnPor} and $\Delta_{\text{o}}^{\text{w}}\phi_{\text{final}}$ were maintained constant at 1.94 nmol·cm^{-2} and −0.25 V, respectively, and $\Delta_{\text{o}}^{\text{w}}\phi_{\text{initial}}$ varied from +0.20 to +0.45 V every 50 mV with a t_{initial} of 30 s (Figure S11a). The current transients measured were near identical for all values of $\Delta_{\text{o}}^{\text{w}}\phi_{\text{initial}}$ tested with no measurable difference in the absorption component and, on close inspection (see inset, Figure S11a), a slight decrease of t_{max} for the prominent nucleation component. This slight increase in the nucleation kinetics is the opposite of what was expected if the film was more compact at positive values of $\Delta_{\text{o}}^{\text{w}}\phi_{\text{final}}$. We attribute the minor increase in nucleation kinetics to an interaction of the organic anions, TB^-, with the ZnPor-IN film at positive potentials leading to a partial opening of the nanostructure. As the ZnPor-IN film and TB^- are both negatively charged, this interaction is far weaker than that of the ZnPor-IN film and the R_2N^+ species. Nevertheless, when the potential is stepped to −0.25 V, slightly less energy is required to open space for the penetration of the R_2N^+ species. In the second experiment, Γ_{ZnPor}, $\Delta_{\text{o}}^{\text{w}}\phi_{\text{initial}}$, and $\Delta_{\text{o}}^{\text{w}}\phi_{\text{final}}$ were maintained constant at 1.94 nmol·cm^{-2}, +0.25, and −0.25 V, respectively, and t_{initial} varied from 5 to 60 s (Figure S11b). As for the previous experiment, the current transients measured were near identical for all values of t_{initial} tested with no measurable difference in the absorption component and, on close inspection (see inset, Figure S11b), a slight increase of t_{max} for the prominent nucleation component. This minor decrease in the nucleation kinetics indicates a slightly more compact nature as t_{initial} increased.

CONCLUSIONS

The thermodynamics and kinetics of ion intercalation into a floating film of zinc porphyrin interfacial nanostructures (ZnPor-INs) were probed electrochemically without the need to support the ZnPor-IN film on a conductive electrode substrate. Instead, the film was supported on an electrified liquid|liquid interface and could be regarded as a mixed-solvent layer separating the aqueous and organic solutions. The electrochemical signal was due to purely ionic processes, not linked to redox reactions.

The film behaves as a capacitor. The ZnPor-IN film is electroneutral and the concentration of free ions is relatively small because of solvation effects. On increasing the negative polarization of the interface, $\Delta_{\text{o}}^{\text{w}}\phi < 0$, the organic ammonium cations (R_2N^+) from the organic phase enter the film and intercalate the ZnPor-IN. Then, a few neutral carboxyl (−COOH) groups are forced to dissociate, and many more transform into $-COOR_2N$. In both cases, the released H^+ ions leave the film and enter the aqueous phase. The charge of the anionic carboxyl groups ($-COO^-$) is mostly compensated for by free R_2N^+ ions. The total (i.e., free and bound) R_2N^+ concentration in the film, $c_{\text{COOR}_2\text{N}} + c_{\text{R}_2\text{N}}^{\text{IN}}$, is a measure of the positive charge accumulated in the film as a capacitor; the negative charge in the capacitor corresponds to H^+ ions leaving the film (where they were bound as −COOH). To a lesser extent, aqueous citrate ($HCit^{2-}$) anions and lithium (Li^+) ions may also participate in this capacitive film behavior.

The shape of the CV was distinctive, formed by the superposition of a narrow peak and a broad peak. The former indicated a positive cooperativity mechanism for ion intercalation and was attributed to structural rearrangements of the porphyrins at the electrified liquid|liquid interface during R_2N^+ intercalation. Employing the Frumkin isotherm, experimental CVs were simulated with negative g interaction parameters in line with those observed for a Li^+ intercalation process, a system with very similar underlying thermodynamics.[13] The kinetics of R_2N^+ intercalation were investigated by potential step chronoamperometry. Depending on the applied interfacial Galvani potential $\Delta_{\text{o}}^{\text{w}}\phi$ and the interfacial concentration Γ_{ZnPor} of ZnPor, current transients presented a decay and multiple nucleation components. The latter was associated with domains where, due to structural rearrangements of the porphyrins, the electrochemically driven binding and ion exchange of R_2N^+ took place faster. The nucleation kinetics were seen to increase as the final potential $\Delta_o^w\phi_{final}$ was set to more negative values and decrease as Γ_{ZnPor} increased.

Overall, using electrified liquid|liquid interfaces, there is clearly significant potential to study, for the time, by electrochemical methodologies the dynamics of ion intercalation into solid matrices that are nonelectronically conductive and/or that operate as nonelectronically connected device components (for example ion-exchange membranes). Such insights may critically influence the performance of a multitude of devices (Li-ion batteries, supercapacitors, fuel cells, electrolyzers, etc.) with energy-related applications.

■ ASSOCIATED CONTENT

Supporting Information

The Supporting Information is available free of charge at https://pubs.acs.org/doi/10.1021/acs.jpcc.0c04976.

> Complete experimental methods (Figures S1 and S2); additional electrochemistry of the floating film of ZnPor-INs at the ITIES (Scheme 1, Figures S3−S7, Tables S1 and S2); further details on modeling the electrochemistry of the floating film of ZnPor-INs at the ITIES (Figure S8 and Tables S3−S5); and further details on the kinetics of structural changes in the ZnPor-IN film during electrochemically driven reversible ion intercalation (Figures S9−S11and Table S6) (PDF)
>
> Mathematica code for Figure 3 (PDF)
>
> Mathematica code for Figures 4 and S8 (PDF)

■ AUTHOR INFORMATION

Corresponding Author

Micheál D. Scanlon − *The Bernal Institute and Department of Chemical Sciences, School of Natural Sciences, University of Limerick (UL), Limerick V94 T9PX, Ireland; Advanced Materials and Bioengineering (AMBER) Centre, Dublin 2, Ireland;* orcid.org/0000-0001-7951-7085;
Email: micheal.scanlon@ul.ie

Authors

Andrés F. Molina-Osorio − *The Bernal Institute and Department of Chemical Sciences, School of Natural Sciences, University of Limerick (UL), Limerick V94 T9PX, Ireland*

José A. Manzanares − *Department of Thermodynamics, Faculty of Physics, University of Valencia, E-46100 Valencia, Spain;* orcid.org/0000-0002-5402-6842

Alonso Gamero-Quijano − *The Bernal Institute and Department of Chemical Sciences, School of Natural Sciences, University of Limerick (UL), Limerick V94 T9PX, Ireland*

Complete contact information is available at:
https://pubs.acs.org/10.1021/acs.jpcc.0c04976

Author Contributions

The manuscript was written through the contributions of all authors.

Notes

The authors declare no competing financial interest.

■ ACKNOWLEDGMENTS

M.D.S. acknowledges the Science Foundation Ireland (SFI) under Grant No. 13/SIRG/2137 and the European Research Council through a Starting Grant (Agreement No. 716792). A.G.-Q. acknowledges funding received from an Irish Research Council Government of Ireland Postdoctoral Fellowship Award (Grant Number GOIPD/2018/252). J.A.M. acknowledges the Ministerio de Ciencia e Innovación (Spain) and the European Regional Development Funds (FEDER), Project No. PGC2018−097359-B-I00.

■ ABBREVIATIONS USED

CV, cyclic voltammogram; IEM, ion-exchange membrane; ITIES, interface between two immiscible electrolyte solutions; PPW, polarizable potential window; PZC, potential of zero charge; ZnPor-INs, zinc porphyrin interfacial nanostructures

■ REFERENCES

(1) Augustyn, V.; McDowell, M. T.; Vojvodic, A. Toward an Atomistic Understanding of Solid-State Electrochemical Interfaces for Energy Storage. *Joule* **2018**, *2*, 2189−2193.

(2) Stamenkovic, V. R.; Strmcnik, D.; Lopes, P. P.; Markovic, N. M. Energy and Fuels from Electrochemical Interfaces. *Nat. Mater.* **2017**, *16*, 57−69.

(3) Bazant, M. Z. Theory of Chemical Kinetics and Charge Transfer Based on Nonequilibrium Thermodynamics. *Acc. Chem. Res.* **2013**, *46*, 1144−1160.

(4) Kuznetsov, A. M.; Ulstrup, J. Theory of Electron Transfer at Electrified Interfaces. *Electrochim. Acta* **2000**, *45*, 2339−2361.

(5) Fong, K. D.; Wang, T.; Smoukov, S. K. Multidimensional Performance Optimization of Conducting Polymer-Based Supercapacitor Electrodes. *Sustainable Energy Fuels* **2017**, *1*, 1857−1874.

(6) Strathmann, H. Electromembrane Processes: Basic Aspects and Applications. In *Comprehensive Membrane Science and Engineering*; Elsevier: 2010; Vol. *2*, pp 391−429.

(7) Strathmann, H.; Grabowski, A.; Eigenberger, G. Electromembrane Processes, Efficient and Versatile Tools in a Sustainable Industrial Development. *Desalination* **2006**, *199*, 1−3.

(8) Peighambardoust, S. J.; Rowshanzamir, S.; Amjadi, M. Review of the Proton Exchange Membranes for Fuel Cell Applications. *Int. J. Hydrogen Energy* **2010**, *35*, 9349−9384.

(9) Yuzer, B.; Selcuk, H.; Chehade, G.; Demir, M. E.; Dincer, I. Evaluation of Hydrogen Production via Electrolysis with Ion Exchange Membranes. *Energy* **2020**, *190*, No. 116420.

(10) Nguyen, T. D.; Whitehead, A.; Wai, N.; Ong, S. J. H.; Scherer, G. G.; Xu, Z. J. Equilibrium and Dynamic Absorption of Electrolyte Species in Cation/Anion Exchange Membranes of Vanadium Redox Flow Batteries. *ChemSusChem* **2019**, *12*, 1076−1083.

(11) Logan, B. E.; Elimelech, M. Membrane-Based Processes for Sustainable Power Generation Using Water. *Nature* **2012**, *488*, 313−319.

(12) Oliot, M.; Galier, S.; Roux de Balmann, H.; Bergel, A. Ion Transport in Microbial Fuel Cells: Key Roles, Theory and Critical Review. *Appl. Energy* **2016**, *183*, 1682−1704.

(13) Levi, M. D. Solid-State Electrochemical Kinetics of Li-Ion Intercalation into Li[Sub 1−x]CoO[Sub 2]: Simultaneous Application of Electroanalytical Techniques SSCV, PITT, and EIS. *J. Electrochem. Soc.* **1999**, *146*, 1279−1289.

(14) Levi, M. D.; Aurbach, D. Frumkin Intercalation Isotherm - a Tool for the Description of Lithium Insertion into Host Materials: A Review. *Electrochim. Acta* **1999**, *45*, 167−185.

(15) Conway, B. E. Two-Dimensional and Quasi-Two-Dimensional Isotherms for Li Intercalation and Upd Processes at Surfaces. *Electrochim. Acta* **1993**, *38*, 1249−1258.

(16) Levi, M. D.; Cohen, Y. S.; Gofer, Y.; Aurbach, D. Electrochemical Responses of Active Metal Insertion Electrodes and Electronically Conducting Polymers: Common Features and New Insights. *Electrochim. Acta* **2004**, *49*, 3701−3710.

(17) Vorotyntsev, M. A.; Daikhin, L. I.; Levi, M. D. Isotherms of Electrochemical Doping and Cyclic Voltammograms of Electroactive Polymer Films. *J. Electroanal. Chem.* **1992**, *332*, 213−235.

(18) Sirisaksoontorn, W.; Lerner, M. M. Preparation of a Homologous Series of Tetraalkylammonium Graphite Intercalation Compounds. *Inorg. Chem.* **2013**, *52*, 7139−7144.

(19) Fogg, A. M.; Dunn, J. S.; Shyu, S.-G.; Cary, D. R.; O'Hare, D. Selective Ion-Exchange Intercalation of Isomeric Dicarboxylate Anions into the Layered Double Hydroxide [LiAl2 (OH) 6] Cl⊙ H2O. *Chem. Mater.* **1998**, *10*, 351−355.

(20) Samec, Z. Electrochemistry at the Interface between Two Immiscible Electrolyte Solutions (IUPAC Technical Report). *Pure Appl. Chem.* **2004**, *76*, 2147−2180.

(21) Peljo, P.; Girault, H. H. Liquid/Liquid Interfaces, Electrochemistry at, Update based on the original article by Frédéric Reymond, Hubert H. Girault, Encyclopedia of Analytical Chemistry, © 2000, John Wiley & Sons, Ltd. *Encycl. Anal. Chem.* **2012**.

(22) Suárez-Herrera, M. F.; Cazade, P.-A.; Thompson, D.; Scanlon, M. D. Monitoring Transient Changes in the Structure of Water at a Polarised Liquid-Liquid Interface Using Electrocapillary Curves. *Electrochem. Commun.* **2019**, *109*, No. 106564.

(23) Suárez-Herrera, M. F.; Scanlon, M. D. On the Non-Ideal Behaviour of Polarised Liquid-Liquid Interfaces. *Electrochim. Acta* **2019**, *328*, No. 135110.

(24) Senthilkumar, S.; Dryfe, R. A. W.; Saraswathi, R. Size-Selective Voltammetry: Modification of the Interface between Two Immiscible Electrolyte Solutions by Zeolite Y. *Langmuir* **2007**, *23*, 3455−3461.

(25) Dryfe, R. A. W.; Holmes, S. M. Zeolitic Rectification of Electrochemical Ion Transfer. *J. Electroanal. Chem.* **2000**, *483*, 144−149.

(26) Lillie, G. C.; Dryfe, R. A. W.; Holmes, S. M. Zeolite-Membrane Modulation of Simple and Facilitated Ion Transfer. *Analyst* **2001**, *126*, 1857−1860.

(27) Jiang, X.; Gao, K.; Hu, D.; Wang, H.; Bian, S.; Chen, Y. Ion-Transfer Voltammetric Determination of Folic Acid at Meso-Liquid-Liquid Interface Arrays. *Analyst* **2015**, *140*, 2823−2833.

(28) Huang, X.; Xie, L.; Lin, X.; Su, B. Permselective Ion Transport Across the Nanoscopic Liquid/Liquid Interface Array. *Anal. Chem.* **2016**, *88*, 6563−6569.

(29) Xie, L.; Huang, X.; Lin, X.; Su, B. Nanoscopic Liquid/Liquid Interface Arrays Supported by Silica Isoporous Membranes: Trans-Membrane Resistance and Ion Transfer Reactions. *J. Electroanal. Chem.* **2017**, *784*, 62−68.

(30) Collins, M. C.; Hébrant, M.; Herzog, G. Ion Transfer at Polarised Liquid-Liquid Interfaces Modified with Adsorbed Silica Nanoparticles. *Electrochim. Acta* **2018**, *282*, 155−162.

(31) Poltorak, L.; Gamero-Quijano, A.; Herzog, G.; Walcarius, A. Decorating Soft Electrified Interfaces: From Molecular Assemblies to Nano-Objects. *Appl. Mater. Today* **2017**, *9*, 533−550.

(32) Stephenson, M. J.; Holmes, S. M.; Dryfe, R. A. W. Electrochemically Controlled Ion Exchange: Proton Exchange with Sodium Zeolite Y. *Angew. Chem., Int. Ed.* **2005**, *44*, 3075−3078.

(33) Stephenson, M. J.; Attfield, M. P.; Holmes, S. M.; Dryfe, R. A. W. Electrochemically Controlled Ion Exchange: Proton Ion Exchange with Sodium Zeolite X and A. *J. Solid State Electrochem.* **2015**, *19*, 1985−1992.

(34) Stephenson, M. J.; Dryfe, R. A. W. Electrochemically Controlled Ion Exchange: Copper Ion Exchange with Sodium Zeolite Y. *Electrochim. Acta* **2007**, *53*, 1182−1188.

(35) Otero, T. F.; Grande, H.-J.; Rodríguez, J. Reinterpretation of Polypyrrole Electrochemistry after Consideration of Conformational Relaxation Processes. *J. Phys. Chem. B* **1997**, *101*, 3688−3697.

(36) Molina-Osorio, A. F.; Cheung, D.; O'Dwyer, C.; Stewart, A. A.; Dossot, M.; Herzog, G.; Scanlon, M. D. Self-Assembly of Porphyrin Nanostructures at the Interface between Two Immiscible Liquids. *J. Phys. Chem. C* **2020**, *124*, 6929−6937.

(37) Monroe, C. W.; Urbakh, M.; Kornyshev, A. A. Understanding the Anatomy of Capacitance at Interfaces between Two Immiscible Electrolytic Solutions. *J. Electroanal. Chem.* **2005**, *582*, 28−40.

(38) Huber, T.; Pecina, O.; Schmickler, W. Influence of the Ions on the Capacity of Liquid | Liquid Interfaces. *J. Electroanal. Chem.* **1999**, *467*, 203−206.

(39) Torrie, G. M.; Valleau, J. P. Double Layer Structure at the Interface between Two Immiscible Electrolyte Solutions. *J. Electroanal. Chem. Interfacial Electrochem.* **1986**, *206*, 69−79.

(40) Yufei, C.; Cunnane, V. J.; Schiffrin, D. J.; Murtomäki, L.; Kontturi, K. Interfacial Capacitance and Ionic Association at Electrified Liquid/Liquid Interfaces. *J. Chem. Soc., Faraday Trans.* **1991**, *87*, 107−114.

(41) Pereira, C. M.; Martins, A.; Rocha, M.; Silva, C. J.; Silva, F. Differential Capacitance of Liquid/Liquid Interfaces: Effect of Electrolytes Present in Each Phase. *J. Chem. Soc. Faraday Trans.* **1994**, *90*, 143−148.

(42) Bates, R. G.; Pinching, G. D. Additions and Corrections-Resolution of the Dissociation Constants of Citric Acid at 0 to 50 Degrees and Determination of Certain Related Thermodynamic Functions. *J. Am. Chem. Soc.* **1949**, *71*, 4165.

(43) Hölzle, M. H.; Retter, U.; Kolb, D. M. The Kinetics of Structural Changes in Cu Adlayers on Au(111). *J. Electroanal. Chem.* **1994**, *371*, 101−109.

(44) Otero, T. F.; Boyano, I. Potentiostatic Oxidation of Polyaniline under Conformational Relaxation Control: Experimental and Theoretical Study. *J. Phys. Chem. B* **2003**, *107*, 4269−4276.

(45) Otero, T. F.; Boyano, I. Comparative Study of Conducting Polymers by the ESCR Model. *J. Phys. Chem. B* **2003**, *107*, 6730−6738.

(46) Nateghi, M. R.; Savabieh, B. Study of Polyaniline Oxidation Kinetics and Conformational Relaxation in Aqueous Acidic Solutions. *Electrochim. Acta* **2014**, *121*, 128−135.

Supporting Information

Electrochemically Controlled Ion Dynamics in Porphyrin Nanostructures

Andrés F. Molina-Osorio,[†] José A. Manzanares,[‡] Alonso Gamero-Quijano[†] and Micheál D. Scanlon*[,†,§]

[†] The Bernal Institute and Department of Chemical Sciences, School of Natural Sciences, University of Limerick (UL), Limerick V94 T9PX, Ireland.
[‡] Department of Thermodynamics, Faculty of Physics, University of Valencia, c/Dr. Moliner, 50, E-46100 Burjasot, Spain.
[§] Advanced Materials and Bioengineering (AMBER) Centre, Ireland.

*E-mail: micheal.scanlon@ul.ie

Table of Contents

Section S1. Experimental Section

S1.1 Materials

All reagents were used as received without further purification. Zinc(II) 5,10,15,20-(tetra-4-carboxyphenyl)porphyrin (ZnPor, ≥ 98%) was purchased from Porphychem. All aqueous solutions were prepared with ultra-pure water (Millipore Milli-Q, resistivity 18.2 MΩ·cm). Bis(triphenylphosphoranylidene)ammonium chloride (R_2NCl, 97% with R = triphenylphosphoranylidene) and lithium tetrakis(pentafluorophenyl)borate diethyletherate ($[Li(OEt_2)]TB$) were obtained from Sigma-Aldrich and Boulder Scientific Company, respectively. Bis(triphenylphosphoranylidene)ammonium tetrakis(pentafluorophenyl)borate (R_2NTB) was prepared by metathesis of equimolar solutions of R_2NCl and $[Li(OEt_2)]TB$ in a methanol-water (2:1 v/v) mixture. The resulting precipitates were filtered, washed, recrystallised from acetone and finally washed 5 times with a methanol-water (2:1 v/v) mixture. Lithium chloride (LiCl, ≥ 99%), lithium hydroxide (LiOH, ≥ 98%), tetraethylammonium chloride (TEACl, ≥ 98%) and citric acid (H_3Cit, ≥ 99.5%) were obtained from Sigma-Aldrich. The organic solvent α,α,α-trifluorotoluene (TFT, ≥ 99%) was obtained from Acros Organics.

S1.2 Functionalising the liquid|liquid interface

Aqueous solutions of ZnPor were prepared by directly dissolving the solid in a lithium citrate (Li_2HCit) buffer pre-adjusted to the desired pH, followed by sonication of the solution for three minutes. Depending on the experiment, the concentration of ZnPor was varied in the range of 10 to 100 μM and the ionic strength of the Li_2HCit buffer solution was maintained at 10 (±2) mM. The selective formation of ZnPor nanostructures at the interface between water and TFT in the four-electrode electrochemical cell was observed upon contacting the ZnPor aqueous solution with the TFT electrolyte. As rationalised in detail recently,[1] self-assembly was observed only at $pH = 5.8 = pK_a(COOH)$, where the ratio between neutral (fully protonated) and tetra-anionic species was close to 1. The self-assembly process was carried out at open circuit potential conditions for 30 min unless stated otherwise. To isolate the ZnPor-INs at the interface, as shown in Figure S1, the upper 50% of the volume of the aqueous phase was carefully removed by a pipette and replaced with porphyrin-free aqueous electrolyte. This procedure was repeated until no porphyrin was detectable in the aqueous phase by UV/vis spectroscopy.

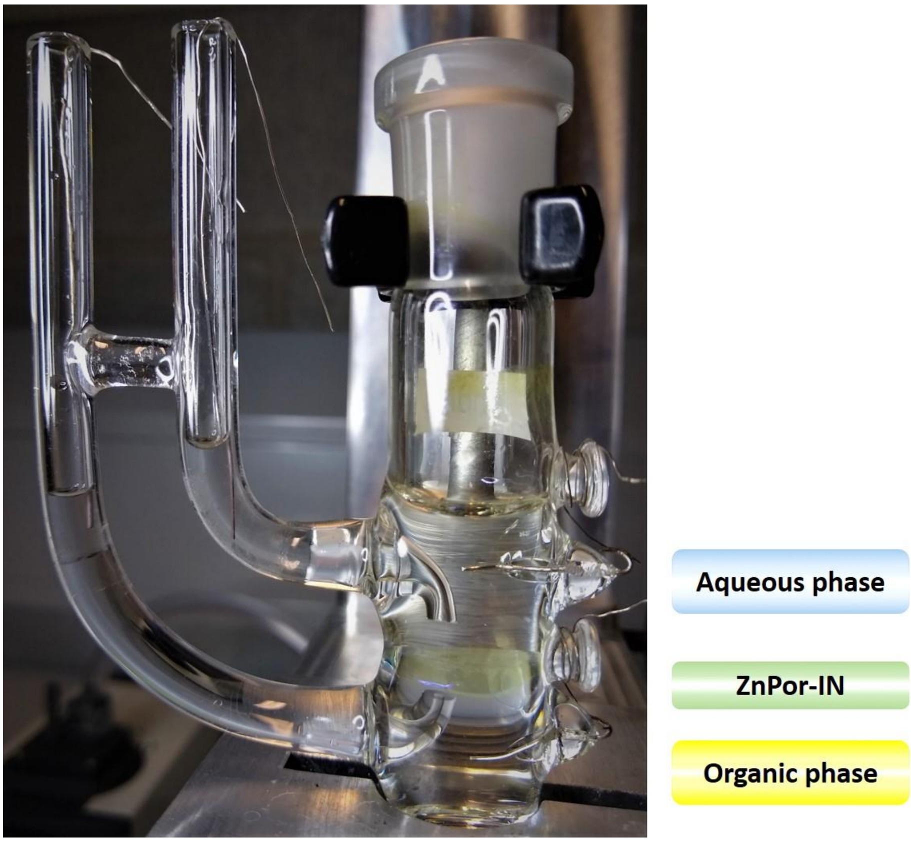

Figure S1. Image of a four-electrode electrochemical cell with the yellow/green ZnPor-IN film floating at the ITIES formed between a Li_2HCit buffered aqueous solution and an organic solution of R_2NTB in TFT (see Scheme 2, main text).

S1.3 Spectroscopic determination of the interfacial concentration Γ_{ZnPor} of ZnPor-INs

The surface concentration Γ_{ZnPor} of the ZnPor-IN was measured following a procedure described recently.[1] Vials containing biphasic systems of ZnPor in lithium citrate buffer (10 mM ionic strength, pH 5.8) at different initial concentrations [ZnPor] in the bulk aqueous phase, and 5 mM R_2NTB in TFT as the organic phase were prepared and left to stand for 30 min. After this time, the porphyrin not adsorbed at the interface was extracted and analysed by UV/vis absorbance spectroscopy to quantify the porphyrin concentration therein (final bulk concentration). By subtracting the final from the initial bulk concentrations, the surface concentration (number of moles adsorbed per geometric area of aqueous|organic interface) was determined. A linear relationship between Γ_{ZnPor} and [ZnPor] was observed as presented in Figure S2a. Quantification of [ZnPor] not adsorbed at the interface was performed using the calibration curve presented in Figure S2b.

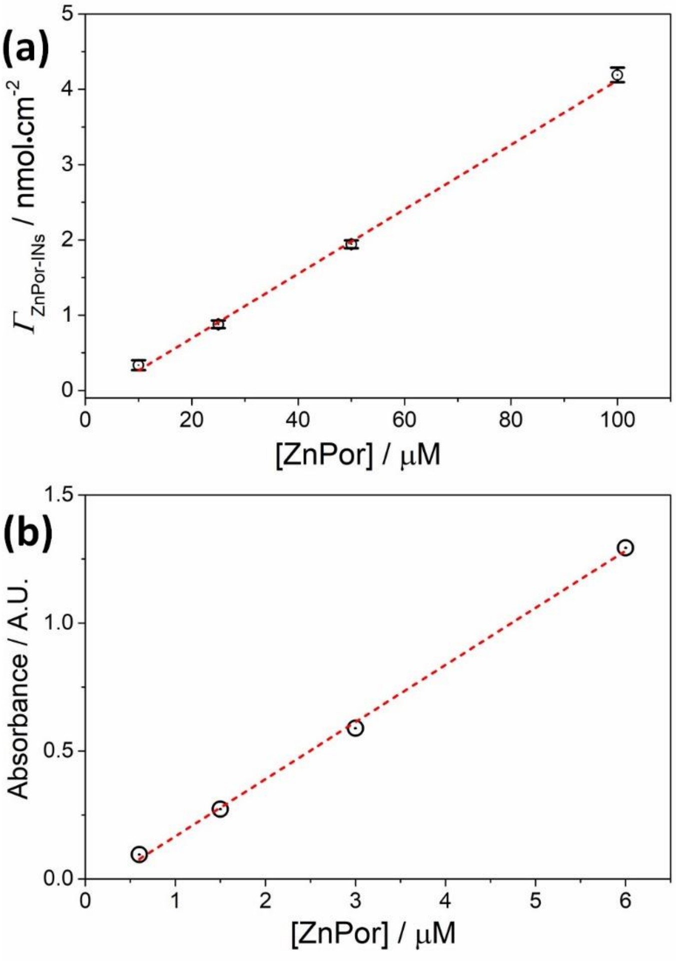

Figure S2. (a) Surface concentration Γ_{ZnPor} of ZnPor-INs as a function of ZnPor concentration [ZnPor] in the bulk aqueous phase. The surface concentration was measured after 30 min of ZnPor self-assembly at pH 5.8 as described in the Experimental Section. (**b**) UV/vis calibration curve used for the quantification of [ZnPor] not adsorbed at the interface. The absorbance was measured at $\lambda_{\max}$ = 422 nm.

S1.4 Electrochemical measurements

Electrochemical experiments at the ZnPor-IN functionalised water-TFT interface were performed using an Autolab PGSTAT204 potentiostat. The general configuration of the biphasic system were outlined in Scheme 2, main text. The four-electrode electrochemical cell had a geometric area of 1.87 cm^2. To supply the current flow, platinum counter electrodes were positioned in the organic and aqueous phases. The potential drop at the liquid|liquid interface was measured by means of a silver/silver citrate (Ag/AgCit) reference electrode immersed in the aqueous phase and a silver/silver chloride (Ag/AgCl) reference electrode immersed in the organic reference solution (an aqueous solution of 10 mM LiCl and 1 mM R_2NCl). Both reference electrodes were connected to the aqueous phase and organic reference solution, respectively, through Luggin capillaries. The organic phase was composed of a highly hydrophobic salt R_2NTB, dissolved in TFT. The aqueous phase consisted of a Li_2HCit solution at different pH values. By introducing a salt in each phase, the interfacial Galvani potential difference $\Delta_{\mathrm{o}}^{\mathrm{w}}\phi$ was varied by external polarisation with a polarisable potential window ranging from –0.3 to +0.6 V. The voltammetry was adjusted to the Galvani potential scale by assuming the formal ion transfer potential of TEA^+ to be 0.149 V.[2]

Cyclic voltammetry and potential step chronoamperometry experiments were performed using *iR* drop compensation (1000 Ω). Differential capacitances at different applied voltages were measured using alternating current voltammetry, also known as potentiodynamic electrochemical impedance spectroscopy, at 80 Hz and assuming the cell behaves as a series R-C circuit. At this frequency, the contribution of Faradaic processes was significant only at the edge of the potential window.

Section S2. Electrochemistry of the floating film of ZnPor-INs at the ITIES

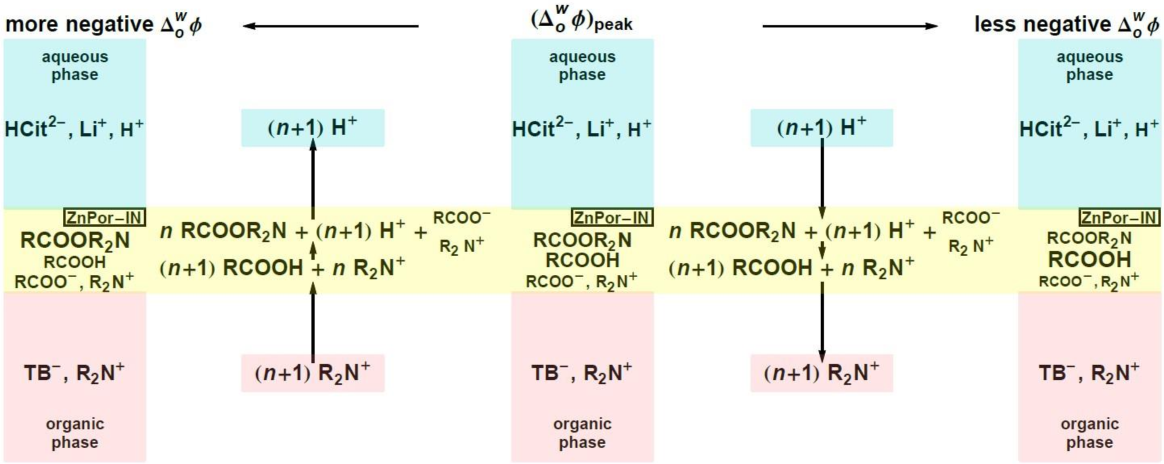

Scheme S1. Detailed schematic of the electrochemically-driven reversible ion intercalation process involving the ZnPor-IN film floating at the electrified liquid|liquid interface, as described in Scheme 1, main text.

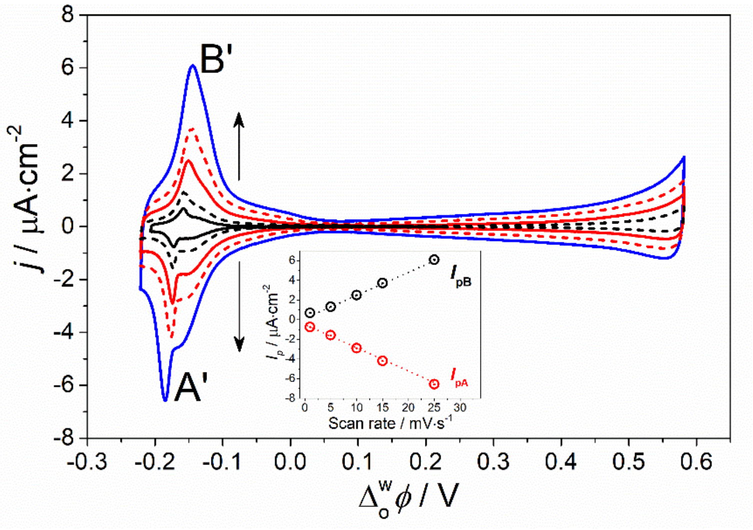

Figure S3. Effect of the scan rate on the electrochemical response of the ZnPor-IN film. The scan rates used were 1, 5, 10, 15 and 25 mV·s^{-1} and Γ_{ZnPor} was 0.34 nmol·cm^{-2}. The electrochemical configuration of the cell was as described in Scheme 2, main text. Inset: the peak current I_p dependence on the scan rate.

Table S1. Analysis of the voltammetric features observed in Figure S3.

Scan rate/(mV·s^{-1})	ΔE_p/mV	Q_A/Q_B
5	19	1.0
10	24	1.0
15	30	0.99
25	40	0.97
50	59	0.96

Table S2. Analysis of the voltammetric features observed in Figure 2b in the main manuscript (data obtained at a scan rate of 1 mV·s^{-1}).

Γ_{ZnPor}/(nmol·cm^{-2})	ΔE_p/mV	Q_A/Q_B
0.34	14	0.75
0.88	18	0.85
1.94	23	0.86
4.19	29	0.89

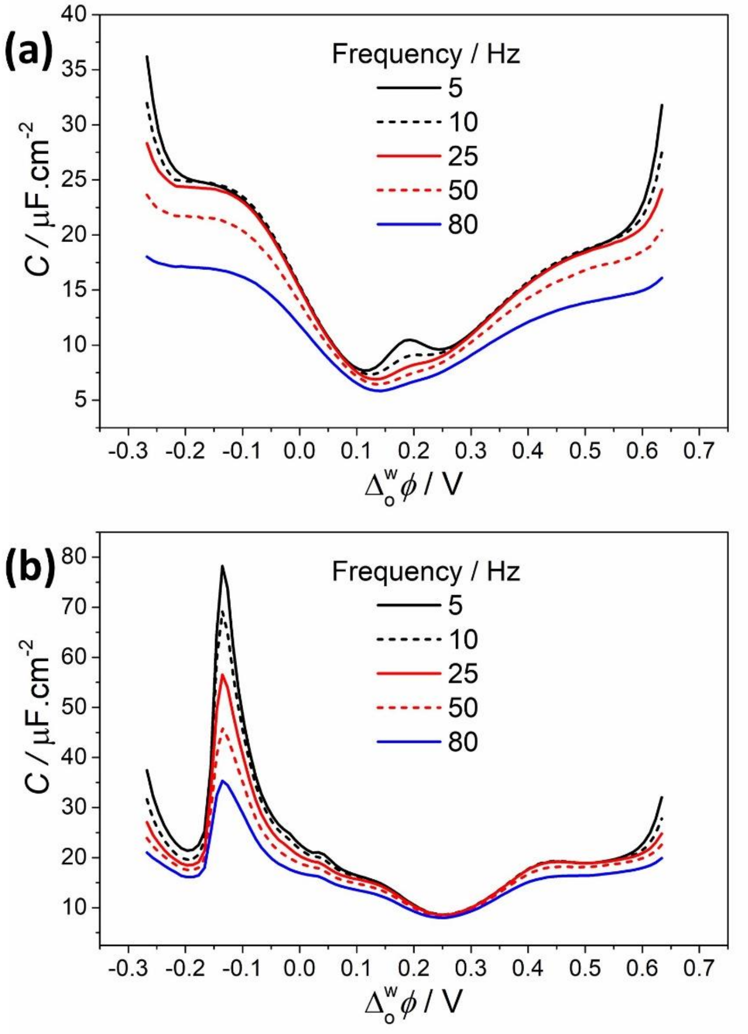

Figure S4. Differential capacitance curves at **(a)** the bare ITIES in the presence of 125 µM of TEACl and 10 mM LiH_2Cit at pH 5.8 in the aqueous phase and **(b)** the ITIES functionalised with a ZnPor-IN film. The capacitance was calculated from impedance measurements every 5 mV at different frequencies assuming an *RC* circuit where *R* represents the solution resistance and *C* the double layer capacitance. The electrochemical configuration of the cell was as described in Scheme 2, main text. Γ_{ZnPor} determined spectroscopically as 0.34 nmol·cm^{-2}.

Figure S4a demonstrates that at 80 Hz the contribution of Faradaic processes was significant only at the edge of the potential window, with the Faradaic ion transfer response of TEA^+ ion transfer entirely filtered out. Meanwhile, in Figure S4b, the peak observed at –0.15 V in the presence of the ZnPor-IN remains, indicating that the latter are associated with adsorption and capacitive processes.

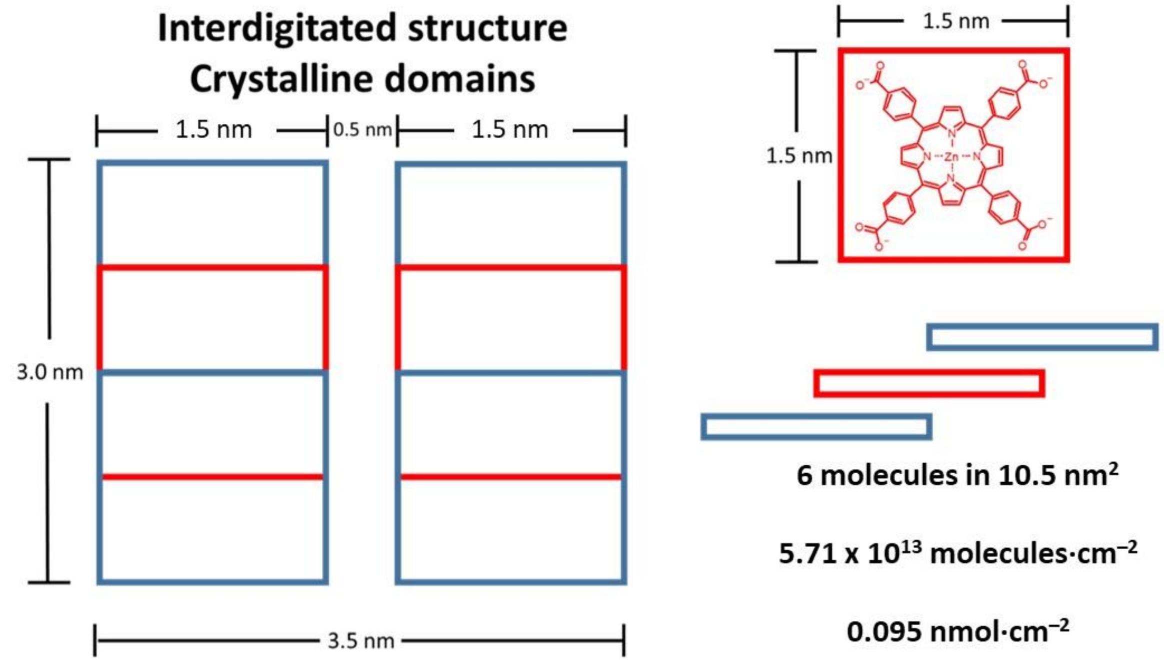

Figure S5. The interdigitated clathrate structure was recently obtained from the XRD analysis of the ZnPor-IN film.[1] The area of a single ZnTPPc molecule is 2.25 nm^2.[3]Assuming perfectly flat lying ZnTPPc molecules in a monolayer and fully crystalline domains of ZnPor-INs in contact with the liquid|liquid interface (*i.e.*, no amorphous domains), the theoretical monolayer concentration of the ZnPor-INs was calculated as $\Gamma_{\mathrm{m}} = 0.095\ \mathrm{nmol{\cdot}cm^{-2}}$ (equivalent to 5.71×10^{13} molecules·cm^{-2}).

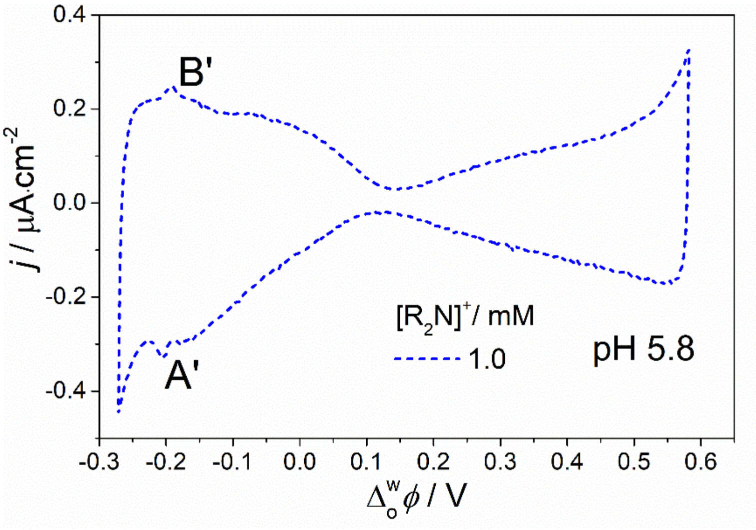

Figure S6. Zoomed version of the CV obtained with [R_2N^+] = 1 mM (dashed blue line in Figure 2d, main text). The scan rate was 5 mV·s^{-1} and Γ_{ZnPor} was 0.34 nmol·cm^{-2}.

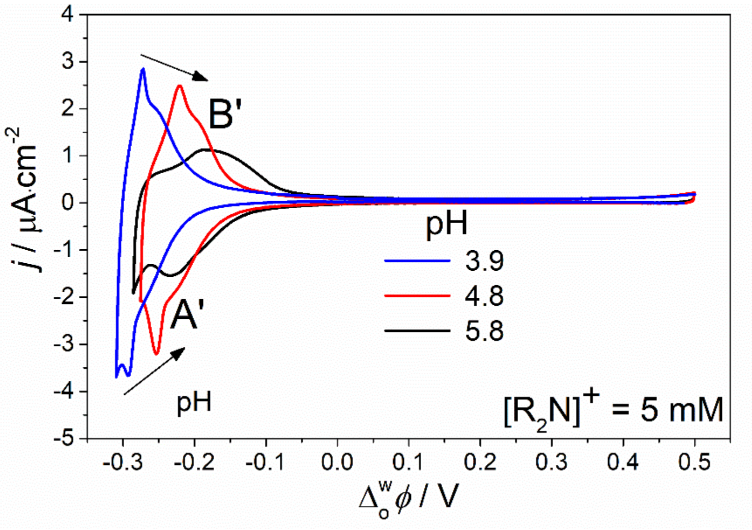

Figure S7. The effect of pH on the electrochemical response was also investigated when the aqueous anion was changed from citrate to chloride. The cell configuration was as described in Scheme 2, main text, with LiCl replacing Li_2HCit. The scan rate was 5 mV·s^{-1} and Γ_{ZnPor} was 0.34 nmol·cm^{-2}.

Section S3. Modelling the electrochemistry of the floating film of ZnPor-INs at the ITIES

S3.1 Distribution equilibrium of the ionic species between phase IN and their bulk phases

The distribution equilibria of the ionic species R_2N^+, TB^-, $HCit^{2-}$, H^+ and Li^+ between phase IN and their respective bulk phases are given by the equality of their electrochemical potentials in these phases, $\tilde{\mu}_{\mathrm{R_2N}}^{\mathrm{o}} = \tilde{\mu}_{\mathrm{R_2N}}^{\mathrm{IN}}$, $\tilde{\mu}_{\mathrm{TB}}^{\mathrm{o}} = \tilde{\mu}_{\mathrm{TB}}^{\mathrm{IN}}$, $\tilde{\mu}_{\mathrm{HCit}}^{\mathrm{w}} = \tilde{\mu}_{\mathrm{HCit}}^{\mathrm{IN}}$, $\tilde{\mu}_{\mathrm{Li}}^{\mathrm{w}} = \tilde{\mu}_{\mathrm{Li}}^{\mathrm{IN}}$ and $\tilde{\mu}_{\mathrm{H}}^{\mathrm{w}} = \tilde{\mu}_{\mathrm{H}}^{\mathrm{IN}}$. Thus, their concentrations in phase IN can be written as

$$c_{\mathrm{R_2N}}^{\mathrm{IN}} = c^{\mathrm{o,b}} P_{\mathrm{R_2N}} \mathrm{e}^{-f\Delta_{\mathrm{o}}^{\mathrm{IN}}\phi} \tag{S1}$$

$$c_{\mathrm{TB}}^{\mathrm{IN}} = c^{\mathrm{o,b}} P_{\mathrm{TB}} \mathrm{e}^{f\Delta_{\mathrm{o}}^{\mathrm{IN}}\phi} \tag{S2}$$

$$c_{\mathrm{HCit}}^{\mathrm{IN}} = c^{\mathrm{w,b}} P_{\mathrm{HCit}} \mathrm{e}^{-2f\Delta_{\mathrm{IN}}^{\mathrm{w}}\phi} \tag{S3}$$

$$c_{\mathrm{H}}^{\mathrm{IN}} = c_{\mathrm{H}}^{\mathrm{w,b}} P_{\mathrm{H}} \mathrm{e}^{f\Delta_{\mathrm{IN}}^{\mathrm{w}}\phi} \tag{S4}$$

$$c_{\mathrm{Li}}^{\mathrm{IN}} = \left(2c^{\mathrm{w,b}} - c_{\mathrm{H}}^{\mathrm{w,b}}\right) P_{\mathrm{Li}} \mathrm{e}^{f\Delta_{\mathrm{IN}}^{\mathrm{w}}\phi} \tag{S5}$$

where $c^{\mathrm{o,b}} = c_{\mathrm{R_2N}}^{\mathrm{o,b}} = c_{\mathrm{TB}}^{\mathrm{o,b}}$ and $c^{\mathrm{w,b}} = c_{\mathrm{HCit}}^{\mathrm{w,b}}$ are the electrolyte concentrations in the bulk organic and aqueous phases, and $f = F/RT$. The pH in the bulk aqueous phase determines the H^+ concentration $c_{\mathrm{H}}^{\mathrm{w,b}}$, and $c_{\mathrm{Li}}^{\mathrm{w,b}} = 2c^{\mathrm{w,b}} - c_{\mathrm{H}}^{\mathrm{w,b}}$. The chemical partition coefficients P_i of the ions are related to their standard transfer potentials and to the Gibbs free energies of transfer,

$$RT\ln P_{\mathrm{R_2N}} = F\Delta_{\mathrm{o}}^{\mathrm{IN}}\phi_{\mathrm{R_2N}}^{\circ} = \mu_{\mathrm{R_2N}}^{\circ,\mathrm{o}} - \mu_{\mathrm{R_2N}}^{\circ,\mathrm{IN}} \tag{S6}$$

$$RT\ln P_{\mathrm{TB}} = -F\Delta_{\mathrm{o}}^{\mathrm{IN}}\phi_{\mathrm{TB}}^{\circ} = \mu_{\mathrm{TB}}^{\circ,\mathrm{o}} - \mu_{\mathrm{TB}}^{\circ,\mathrm{IN}} \tag{S7}$$

$$RT\ln P_{\mathrm{HCit}} = 2F\Delta_{\mathrm{IN}}^{\mathrm{w}}\phi_{\mathrm{HCit}}^{\circ} = \mu_{\mathrm{HCit}}^{\circ,\mathrm{w}} - \mu_{\mathrm{HCit}}^{\circ,\mathrm{IN}} \tag{S8}$$

$$RT\ln P_{\mathrm{H}} = -F\Delta_{\mathrm{IN}}^{\mathrm{w}}\phi_{\mathrm{H}}^{\circ} = \mu_{\mathrm{H}}^{\circ,\mathrm{w}} - \mu_{\mathrm{H}}^{\circ,\mathrm{IN}} \tag{S9}$$

$$RT\ln P_{\mathrm{Li}} = -F\Delta_{\mathrm{IN}}^{\mathrm{w}}\phi_{\mathrm{Li}}^{\circ} = \mu_{\mathrm{Li}}^{\circ,\mathrm{w}} - \mu_{\mathrm{Li}}^{\circ,\mathrm{IN}} \tag{S10}$$

where $\mu_i^{\circ,\varphi}$ is the standard chemical potential of ionic species *i* in phase φ.

The ion exchange reaction, Equation (7), main text, can be considered as the combination of the acid dissociation

$$-\mathrm{COOH(IN)} \rightleftarrows -\mathrm{COO^-(IN)} + \mathrm{H^+(IN)} \tag{S11}$$

and the binding or adsorption reaction

$$-\mathrm{COO^-(IN)} + \mathrm{R_2N^+(IN)} \rightleftarrows -\mathrm{COOR_2N(IN)}\ . \tag{S12}$$

Hence, the ion exchange equilibrium constant can be considered the product of the acid dissociation constant $K_{\mathrm{a}}^{\mathrm{IN}}$ and the R_2N^+ binding constant $K_{\mathrm{b}}^{\mathrm{IN}}$,

$$K_{\mathrm{IE}}^{\circ,\mathrm{IN}} = K_{\mathrm{a}}^{\mathrm{IN}} K_{\mathrm{b}}^{\mathrm{IN}} c^{\circ}. \tag{S13}$$

These constants are defined by the standard reaction Gibbs energies,

$$\Delta G_{\mathrm{IE}}^{\circ,\mathrm{IN}} = -RT\ln K_{\mathrm{IE}}^{\circ,\mathrm{IN}} = \mu_{\mathrm{COOR_2N}}^{\circ} + \mu_{\mathrm{H}}^{\circ,\mathrm{IN}} - \mu_{\mathrm{COOH}}^{\circ} - \mu_{\mathrm{R_2N}}^{\circ,\mathrm{IN}} \tag{S14}$$

$$\Delta G_{\mathrm{a}}^{\circ,\mathrm{IN}} = -RT\ln K_{\mathrm{a}}^{\mathrm{IN}} = \mu_{\mathrm{COO^-}}^{\circ} + \mu_{\mathrm{H}}^{\circ,\mathrm{IN}} - \mu_{\mathrm{COOH}}^{\circ} \tag{S15}$$

$$\Delta G_{\mathrm{b}}^{\circ,\mathrm{IN}} = -RT\ln K_{\mathrm{b}}^{\mathrm{IN}} = \mu_{\mathrm{COOR_2N}}^{\circ} - \mu_{\mathrm{COO^-}}^{\circ} - \mu_{\mathrm{R_2N}}^{\circ,\mathrm{IN}} \quad . \tag{S16}$$

Using the above equilibrium conditions, the electroneutrality condition (Equation (2), main text) can be written as an equation in the variable $y = \mathrm{e}^{f\Delta_{\mathrm{IN}}^{\mathrm{w}}\phi}$,

$$\frac{K_{\mathrm{a}}^{\mathrm{IN}} c^{\circ} c_{\mathrm{T,COO}}}{K_{\mathrm{a}}^{\mathrm{IN}} c^{\circ} + \left(c_{\mathrm{H}}^{\mathrm{w,b}} P_{\mathrm{H}} + K_{\mathrm{IE}}^{\circ,\mathrm{IN}} c^{\mathrm{o,b}} P_{\mathrm{R_2N}} \mathrm{e}^{-f\Delta_{\mathrm{o}}^{\mathrm{w}}\phi}\right) y} = 2c^{\mathrm{w,b}}\left(P_{\mathrm{Li}} y - P_{\mathrm{HCit}} y^{-2}\right)$$
$$+c^{\mathrm{o,b}}\left(P_{\mathrm{R_2N}} \mathrm{e}^{-f\Delta_{\mathrm{o}}^{\mathrm{w}}\phi} y - P_{\mathrm{TB}} \mathrm{e}^{f\Delta_{\mathrm{o}}^{\mathrm{w}}\phi} y^{-1}\right) + c_{\mathrm{H}}^{\mathrm{w,b}}\left(P_{\mathrm{H}} - P_{\mathrm{Li}}\right) y \tag{S17}$$

whose numerical solution allows the determination of the potential drop $\Delta_{\mathrm{IN}}^{\mathrm{w}}\phi = (RT/F)\ln y$. In the case of negligible $c_{\mathrm{COO^-}}^{\mathrm{IN}}$ and very negative $\Delta_{\mathrm{o}}^{\mathrm{w}}\phi$, Equation (S17) reduces to $2c_{\mathrm{HCit}}^{\mathrm{IN}} = c_{\mathrm{R_2N}}^{\mathrm{IN}}$, *i.e.*, $2c^{\mathrm{w,b}} P_{\mathrm{HCit}} y^{-2} = c^{\mathrm{o,b}} P_{\mathrm{R_2N}} \mathrm{e}^{-f\Delta_{\mathrm{o}}^{\mathrm{w}}\phi} y$, which provides a convenient initial guess

$$y_0 = \mathrm{e}^{f\Delta_{\mathrm{o}}^{\mathrm{w}}\phi/3} \left(\frac{2c^{\mathrm{w,b}} P_{\mathrm{HCit}}}{c^{\mathrm{o,b}} P_{\mathrm{R_2N}}}\right)^{1/3} \tag{S18}$$

to solve Equation (S17). That is, $\Delta_{\mathrm{IN}}^{\mathrm{w}}\phi$ is then close to one third of $\Delta_{\mathrm{o}}^{\mathrm{w}}\phi$.

S3.2 Simulating CVs

The CVs can be simulated using an equivalent electrical circuit consisting of the solution resistance R_{sol} in series with the parallel combination of the film capacitance *C* and the charge transfer resistance R_{ct}. The potential applied to this equivalent circuit during a CV scan is

$$\Delta_{\mathrm{o}}^{\mathrm{w}}\phi(t) = \varepsilon_{\mathrm{f}} + \nu\,|t_{\max} - t|, \quad (0 \le t \le 2t_{\max}) \tag{S19}$$

where $t_{\max} = (\varepsilon_{\mathrm{i}} - \varepsilon_{\mathrm{f}})/\nu$ and ν is the scan rate ($\nu = -\mathrm{d}\Delta_{\mathrm{o}}^{\mathrm{w}}\phi/\mathrm{d}t$ for $0 \le t \le t_{\max}$). The potential drop across *C* and R_{ct} is denoted as $\varepsilon_{\mathrm{c}}(t)$. Note that *C* is a function of this potential, Equation (10), main text. The sum of the current $\varepsilon_{\mathrm{c}}(t)/R_{\mathrm{ct}}$ across R_{ct} and the pseudo-capacitive current $\mathrm{d}q^{\mathrm{o}}/\mathrm{d}t = C\mathrm{d}\varepsilon_{\mathrm{c}}/\mathrm{d}t$ across *C* is the observed current density $j(t) = (\Delta_{\mathrm{o}}^{\mathrm{w}}\phi - \varepsilon_{\mathrm{c}})/R_{\mathrm{sol}}$,

$$\frac{\Delta_{\mathrm{o}}^{\mathrm{w}}\phi(t) - \varepsilon_{\mathrm{c}}(t)}{R_{\mathrm{sol}}} = \frac{\varepsilon_{\mathrm{c}}(t)}{R_{\mathrm{ct}}} + C(\varepsilon_{\mathrm{c}}(t))\frac{\mathrm{d}\varepsilon_{\mathrm{c}}}{\mathrm{d}t}\,. \tag{S20}$$

The solution of this equation in $\varepsilon_{\mathrm{c}}(t)$, with the initial condition $\varepsilon_{\mathrm{c}}(0) = \varepsilon_{\mathrm{i}}$, allows us to evaluate $j(t)$. The key feature of these CVs is the "adsorption" current $j \approx \mathrm{d}q^{\mathrm{o}}/\mathrm{d}t \approx C\nu$. The small difference in the peak potentials of the forward and backward scans is mainly determined by R_{sol}.

S3.3 Frumkin binding isotherm

The equilibrium condition for the R$_2$N$^+$ adsorption reaction (S12) is $\mu_{\mathrm{COOR_2N}} = \mu_{\mathrm{COO^-}} + \mu_{\mathrm{R_2N}}^{\mathrm{IN}}$ and can also be presented as

$$\frac{c_{\mathrm{COOR_2N}}}{c_{\mathrm{COOH}}+c_{\mathrm{COO^-}}} = \frac{\theta}{1-\theta} = \frac{K_{\mathrm{IE}}^{\circ,\mathrm{IN}} c_{\mathrm{R_2N}}^{\mathrm{IN}}}{K_{\mathrm{a}}^{\mathrm{IN}} c^{\circ} + c_{\mathrm{H}}^{\mathrm{IN}}} \tag{S21}$$

$$\frac{c_{\mathrm{COOR_2N}}}{c_{\mathrm{COO^-}}} = \frac{\theta}{1-\theta}\frac{1}{\alpha} = K_{\mathrm{b}}^{\mathrm{IN}} c_{\mathrm{R_2N}}^{\mathrm{IN}} \tag{S22}$$

where $\theta = c_{\mathrm{COOR_2N}}/c_{\mathrm{T,COO}}$ is the fraction of sites occupied by R$_2$N$^+$ ions, α is the degree of acid dissociation defined by $\alpha/(1-\alpha) = c_{\mathrm{COO^-}}/c_{\mathrm{COOH}}$, and we have used Equations (6), main text, and (S13). When the species –COOR$_2$N interact, their chemical potential is

$$\mu_{\mathrm{COOR_2N}} = \mu_{\mathrm{COOR_2N}}^{\circ} + RT\ln\theta + gRT\theta, \tag{S23}$$

and the Frumkin isotherm

$$\frac{\theta}{1-\theta}\mathrm{e}^{g\theta} = \alpha K_{\mathrm{b}}^{\mathrm{IN}} c_{\mathrm{R_2N}}^{\mathrm{IN}} = \frac{K_{\mathrm{IE}}^{\circ,\mathrm{IN}} c_{\mathrm{R_2N}}^{\mathrm{IN}}}{K_{\mathrm{a}}^{\mathrm{IN}} c^{\circ} + c_{\mathrm{H}}^{\mathrm{IN}}} = \frac{K_{\mathrm{IE}}^{\circ,\mathrm{IN}} c^{\mathrm{o,b}} P_{\mathrm{R_2N}} \mathrm{e}^{-f\Delta_{\mathrm{o}}^{\mathrm{w}}\phi} \mathrm{e}^{f\Delta_{\mathrm{IN}}^{\mathrm{w}}\phi}}{K_{\mathrm{a}}^{\mathrm{IN}} c^{\circ} + c_{\mathrm{H}}^{\mathrm{w,b}} P_{\mathrm{H}} \mathrm{e}^{f\Delta_{\mathrm{IN}}^{\mathrm{w}}\phi}} \tag{S24}$$

should then be used to describe the cooperative adsorption of R$_2$N$^+$ ions, *i.e.*, the equilibrium of reaction (S12).

Using a lattice model and the mean-field approximation, the interaction energy between adsorbed R$_2$N$^+$ ions is estimated as $E = (1/2)z_{\mathrm{c}}\varepsilon N^2/N_{\mathrm{s}}$, where N_{s} is the number of lattice sites, z_{c} is the coordination number (*i.e.*, the number of nearest neighbours), *N* is the number of adsorbed ions, and ε is the molar interaction energy between ions adsorbed in neighbouring sites. Thence, the chemical potential of species –COOR$_2$N is given by Equation (S23). Negative values of $g = z_{\mathrm{c}}\varepsilon/RT$ correspond to attractive interactions between adsorbed ions, which reduce $\mu_{\mathrm{COOR_2N}}$, and to positive cooperativity. When $g \leq -4$, *i.e.*, for temperatures below the critical one, $T_{\mathrm{c}} = -z_{\mathrm{c}}\varepsilon/4R > 0$, phase transitions can occur and to avoid unrealistic predictions, the grand canonical ensemble should then be used to deduce the adsorption isotherm.[4]

If the Frumkin adsorption model is used then $K_{\mathrm{IE}}^{\circ,\mathrm{IN}}\mathrm{e}^{-g\theta}$ should replace $K_{\mathrm{IE}}^{\circ,\mathrm{IN}}$ in Equations (8), (9) and (11) in the main text. For instance, Equation (9) becomes

$$\frac{c_{\mathrm{COO^-}}}{c_{\mathrm{T,COO}}}=\frac{K_{\mathrm{a}}^{\mathrm{IN}}c^{\circ}}{K_{\mathrm{a}}^{\mathrm{IN}}c^{\circ}+c_{\mathrm{H}}^{\mathrm{IN}}+K_{\mathrm{IE}}^{\circ,\mathrm{IN}}\mathrm{e}^{-g\theta}c_{\mathrm{R_2N}}^{\mathrm{IN}}}\ . \qquad \text{(S25)}$$

The system formed by Equations (S24) and (S17), with $K_{\mathrm{IE}}^{\circ,\mathrm{IN}}\mathrm{e}^{-g\theta}$ replacing $K_{\mathrm{IE}}^{\circ,\mathrm{IN}}$ in the latter, must be simultaneously solved to determine the unknowns $\Delta_{\mathrm{IN}}^{\mathrm{w}}\phi$ and θ as functions of $\Delta_{\mathrm{o}}^{\mathrm{w}}\phi$, for given values of $c^{\mathrm{o,b}}$, $c^{\mathrm{w,b}}$ and $c_{\mathrm{H}}^{\mathrm{w,b}}$. Then, the capacitance C is calculated with Equation (10), main text, and the CV is simulated with Equation (S20).

S3.4 Relations between the equilibrium constants in different phases

The equilibrium constant of the acid-dissociation reaction

$$-\mathrm{COOH(IN)} \rightleftarrows -\mathrm{COO^-(IN)}+\mathrm{H^+(w)} \qquad \text{(S26)}$$

is the acidity constant $K_{\mathrm{a}}=10^{-5.8}$, and the standard Gibbs energy of reaction is

$$\Delta G_{\mathrm{a}}^{\circ}=-RT\ln K_{\mathrm{a}}=\mu_{\mathrm{COO^-}}^{\circ}+\mu_{\mathrm{H^+}}^{\circ,\mathrm{w}}-\mu_{\mathrm{COOH}}^{\circ}\ . \qquad \text{(S27)}$$

The equilibrium constant of the binding reaction

$$-\mathrm{COO^-(IN)}+\mathrm{R_2N^+(o)} \rightleftarrows -\mathrm{COOR_2N(IN)} \qquad \text{(S28)}$$

is the (intrinsic) binding constant K_{b} which is implicitly defined as

$$\Delta G_{\mathrm{b}}^{\circ}=-RT\ln K_{\mathrm{b}}=\mu_{\mathrm{COOR_2N}}^{\circ}-\mu_{\mathrm{COO^-}}^{\circ}-\mu_{\mathrm{R_2N}}^{\circ,\mathrm{o}}\ . \qquad \text{(S29)}$$

The equilibrium constant of the ion exchange reaction

$$-\mathrm{COOH(IN)}+\mathrm{R_2N^+(o)} \rightleftarrows -\mathrm{COOR_2N(IN)}+\mathrm{H^+(w)} \qquad \text{(S30)}$$

is the (intrinsic) ion exchange constant K_{IE}° which is implicitly defined as

$$\Delta G_{\mathrm{IE}}^{\circ}=-RT\ln K_{\mathrm{IE}}^{\circ}=\mu_{\mathrm{COOR_2N}}^{\circ}+\mu_{\mathrm{H}}^{\circ,\mathrm{w}}-\mu_{\mathrm{COOH}}^{\circ}-\mu_{\mathrm{R_2N}}^{\circ,\mathrm{o}}\ . \qquad \text{(S31)}$$

Its relation with the acidity and the binding constants is $K_{\mathrm{IE}}^{\circ}=K_{\mathrm{a}}K_{\mathrm{b}}c^{\circ}$.

Similarly, in the ZnPor-IN film (phase IN), the equilibrium constant of reaction (S11) is

$$K_{\mathrm{a}}^{\mathrm{IN}}=K_{\mathrm{a}}P_{\mathrm{H}}\ . \qquad \text{(S32)}$$

The equilibrium constant of reaction (S12) is defined through Eq. (S16) and its relation to that in bulk phase is

$$K_{\mathrm{b}}^{\mathrm{IN}}=K_{\mathrm{b}}/P_{\mathrm{R_2N}}\ . \qquad \text{(S33)}$$

The equilibrium constant of the ion exchange reaction in the film, Equation (7) in the main text, is defined through Eq. (S14) and its relation to that in bulk phase is $K_{\mathrm{IE}}^{\circ,\mathrm{IN}} = K_{\mathrm{a}}^{\mathrm{IN}} K_{\mathrm{b}}^{\mathrm{IN}} c^{\circ} = K_{\mathrm{IE}}^{\circ} P_{\mathrm{H}} / P_{\mathrm{R_2N}}$. That is, the solvation effects on ion partitioning also affect the binding constant and the ion exchange equilibrium constant.

S3.5 Mathematica code to simulate the CVs in the presence of the ZnPor-IN film

Files available free of charge on the ACS Publications website.

Table S3. Parameter values for the simulated CVs in Figure 3a, main text. The chemical partition coefficient is $P_i = 3 \times 10^{-4}$ for all ionic species (i = R_2N^+, TB^-, $HCit^{2-}$, H^+, Li^+) and $\mathrm{p}K_{\mathrm{b}} = -\lg K_{\mathrm{b}} = -\lg\left(K_{\mathrm{b}}^{\mathrm{IN}} P_{\mathrm{R_2N}}\right)$.

Γ_{ZnPor} /(nmol·cm^{-2})	$c_{\mathrm{T,COO}}$/mM	pK_{b}	R_{sol}/(kΩ·cm^2)	R_{ct}/(MΩ·cm^2)
0.34	42	3.3	4.5	3.5
0.88	100	3.3	4.5	2.0
1.94	214	3.1	2.8	2.0
4.19	416	3.1	1.4	2.0

Table S4. Parameter values for the simulated CVs in Figures 3b and c, main text. As shown in Table S3, $c_{\mathrm{T,COO}}$ = 42 mM because Γ_{ZnPor} = 0.34 nmol·cm^{-2}. The chemical partition coefficient is $P_i = 3 \times 10^{-4}$ for all ionic species (i = R_2N^+, TB^-, $HCit^{2-}$, H^+, Li^+).

pH	$c^{\mathrm{o,b}}$/mM	pK_{b}	R_{sol}/(kΩ·cm^2)	R_{ct}/(MΩ·cm^2)
5.8	5.0	3.50	4.0	3.0
5.0	5.0	3.55	4.0	3.5
4.5	5.0	3.65	4.0	2.5
4.0	5.0	3.65	4.0	2.5
3.0	5.0	3.65	4.0	2.5
5.8	5.0	3.60	2.8	3.0
5.8	2.5	3.40	2.8	3.0
5.8	1.0	3.60	2.8	3.0

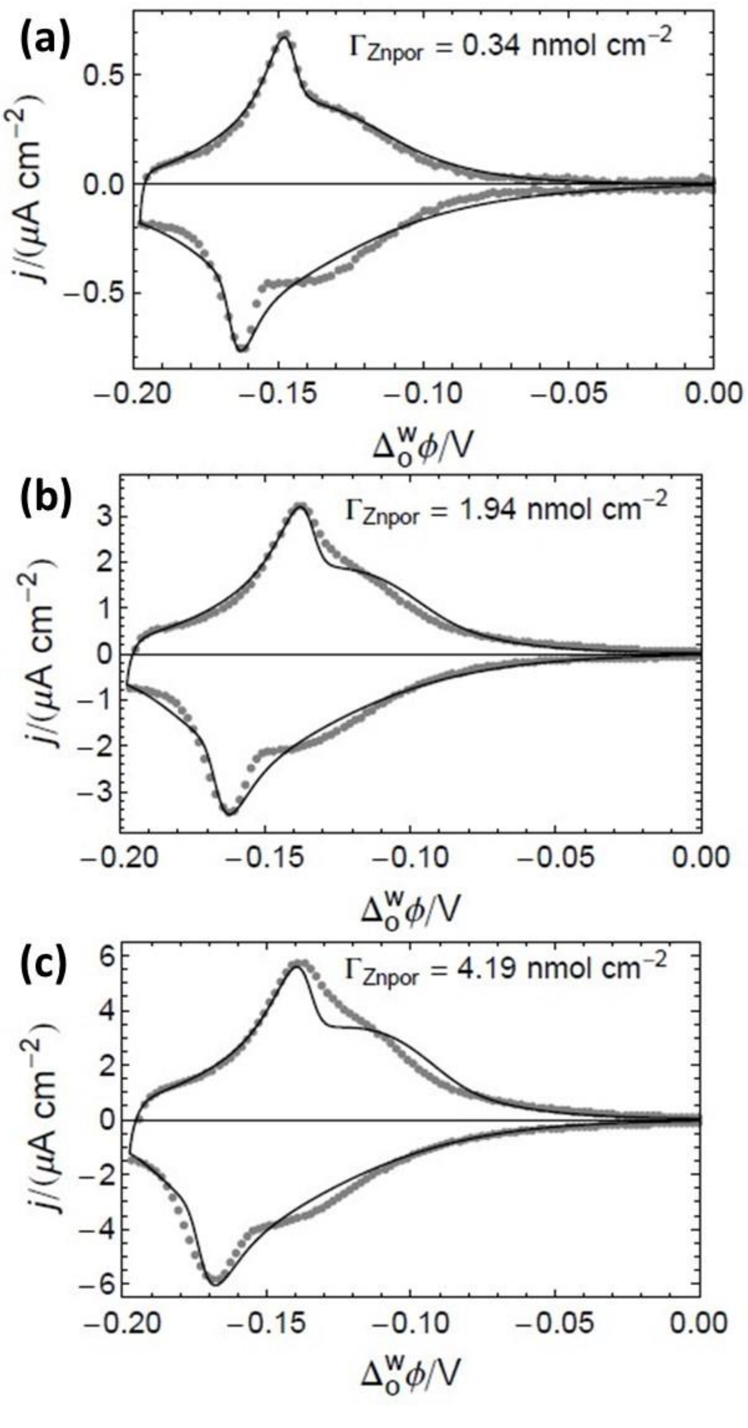

Figure S8. The consideration of two types of binding sites, described by Equation (S24) with $g_{\mathrm{narrow}} = -3.5$ and $g_{\mathrm{broad}} = -0.7$, predicts simulated CVs (lines) at 1 mV·s^{-1} that resemble more closely the experimental observations (symbols). Comparisons are provided for CVs obtained with Γ_{ZnPor} values of 0.34, 1.94 and 4.19 nmol·cm^{-2}. The parameter values (see Table S5) have been chosen on the basis of a qualitative agreement and not using a fitting algorithm.

Table S5. Parameter values for the simulated CVs in Figures 4, main text, and S7. The partition coefficient is $P_i = 3 \times 10^{-5}$ for all ionic species (i = R_2N^+, TB^-, $HCit^{2-}$, H^+, Li^+). The values of $\mathrm{p}K_\mathrm{b} = -\lg K_\mathrm{b} = -\lg\left(K_\mathrm{b}^\mathrm{IN} P_{\mathrm{R_2N}}\right)$ are shown. The carboxyl groups responsible for the narrow peak have a more negative Frumkin parameter $g_\mathrm{narrow} = -3.5$ and a smaller binding constant $K_\mathrm{b,narrow}$, so that the narrow peak appears at more negative $\Delta_\mathrm{o}^\mathrm{w}\phi$, compared to the broad peak with $g_\mathrm{broad} = -0.7$ and larger $K_\mathrm{b,broad}$.

Γ_ZnPor /(nmol·cm^{-2})	$c_\mathrm{T,COO}^\mathrm{narrow}$/mM	$c_\mathrm{T,COO}^\mathrm{broad}$/mM	$\mathrm{p}K_\mathrm{b}^\mathrm{narrow}$	$\mathrm{p}K_\mathrm{b}^\mathrm{broad}$	R_sol/(kΩ·cm^2)	R_ct/(MΩ·cm^2)
0.34	10	31	4.04	3.30	13	7
0.88	24	70	4.13	3.40	8	5
1.94	46	160	3.98	3.20	5.4	4
4.19	84	295	4.05	3.20	3.7	10

Section S4. The kinetics of structural changes in the ZnPor-IN film during electrochemically-driven reversible ion intercalation

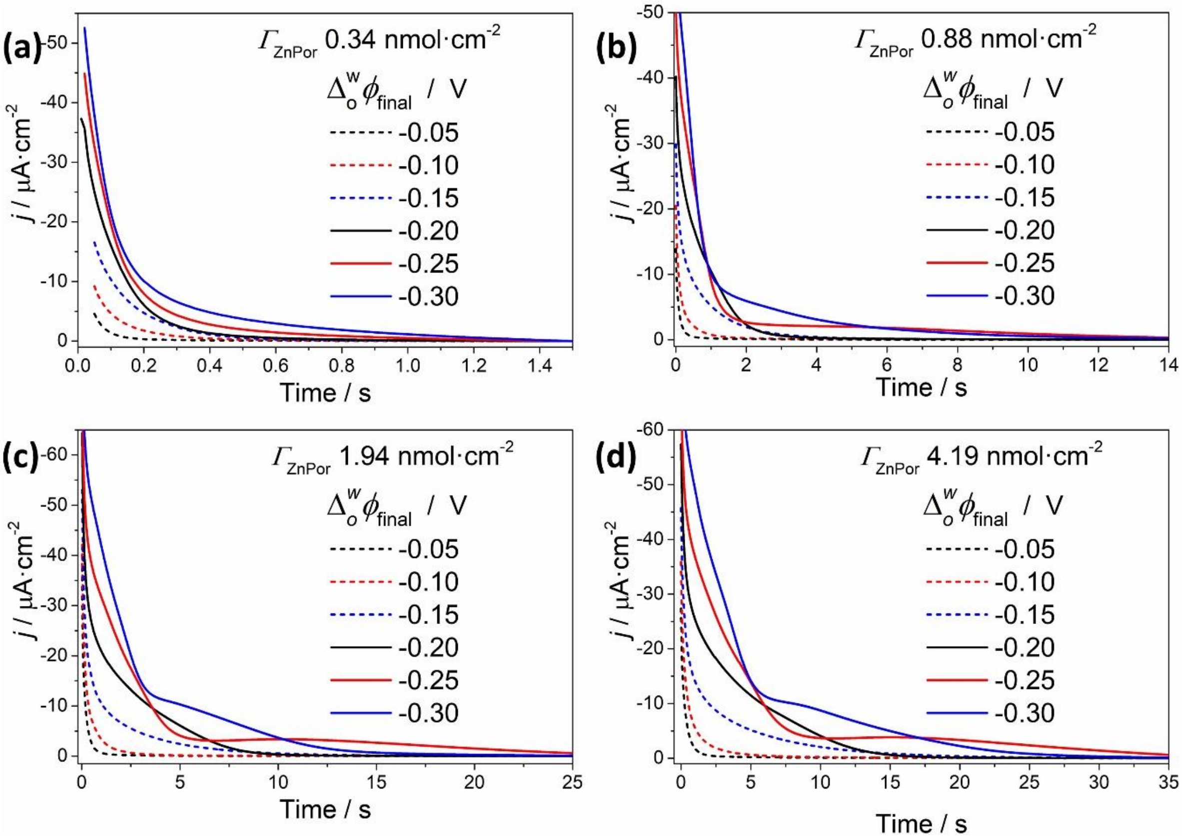

Figure S9. Current transients probing the influence of $\Delta_o^w\phi_{final}$ were obtained by varying $\Delta_o^w\phi_{final}$ in 50 mV increments at a constant $\Delta_o^w\phi_{initial}$ of +0.25 V for 30 s ($t_{initial}$) with Γ_{ZnPor} values of **(a)** 0.34, **(b)** 0.88, **(c)** 1.94 and **(d)** 4.19 nmol·cm^{-2}, respectively.

Table S6. All t_{max} values in Table S6 were obtained from the derivative of current transients obtained in the presence of the ZnPor-IN film as a function of both Γ_{ZnPor} and $\Delta_{\mathrm{o}}^{\mathrm{w}}\phi_{\mathrm{initial}}$ with a constant $\Delta_{\mathrm{o}}^{\mathrm{w}}\phi_{\mathrm{initial}}$ of +0.25 V for 30 s (t_{initial}).

Γ_{ZnPor}/(nmol·cm^{-2})	t_{max1}/s			t_{max2}/s			t_{max3}/s		
	–0.25 V	–0.30 V	–0.35 V	–0.25 V	–0.30 V	–0.35 V	–0.25 V	–0.30 V	–0.35 V
0.34	0.43	0.27	-	-	0.51	0.50	-	-	-
0.88	0.75	0.08	1.31	-	0.33	3.29	-	1.71	-
1.94	1.03	0.7	0.66	2.87	1.73	1.3	-	10.22	4.5
4.19	1.81	1.14	0.85	4.86	2.82	2.1	-	15.21	8.13

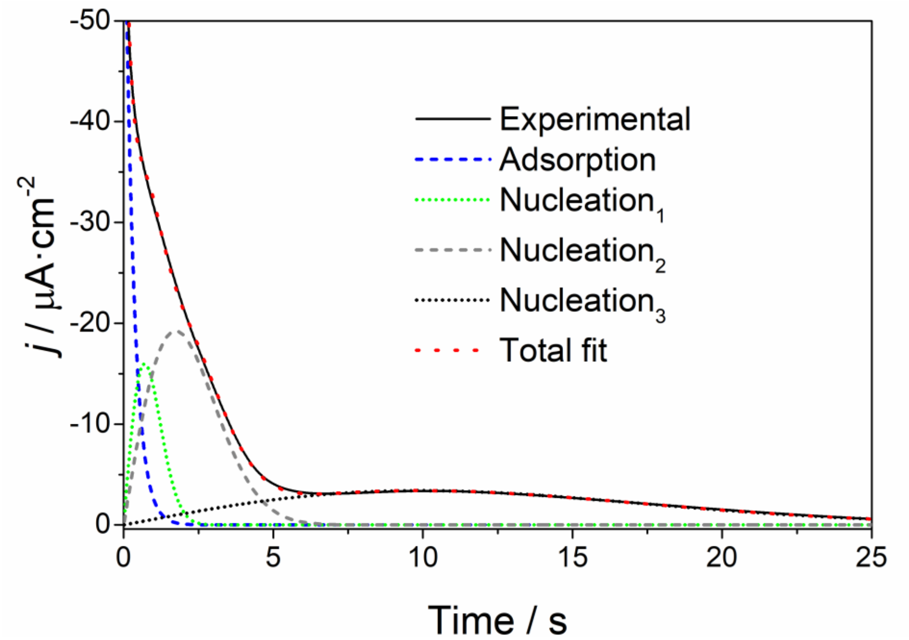

Figure S10. Using the t_{max} values outlined in Table S6 obtained from the derivative of each current transient, the total fitted current for any transient may be obtained as a summation of the adsorption and three nucleation components using exponential decay and Gaussian-type functions, respectively. In this example, the current transient fitted (dotted red line) is that obtained experimentally (solid black line) with a Γ_{ZnPor} of 1.94 nmol·cm^{-2}, $\Delta_{\mathrm{o}}^{\mathrm{w}}\phi_{\mathrm{initial}}$ of +0.25 V for 30 s, and $\Delta_{\mathrm{o}}^{\mathrm{w}}\phi_{\mathrm{final}}$ of –0.25 V.

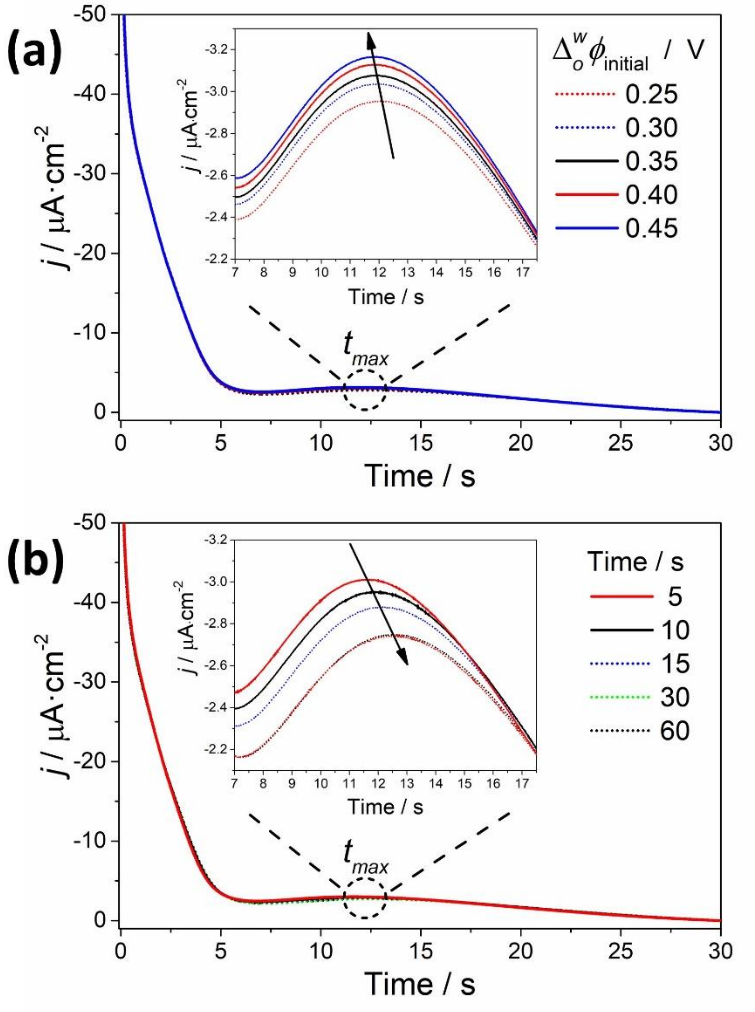

Figure S11. (a) Current transients probing the influence of $\Delta_o^w\phi_{\text{initial}}$ were obtained at a constant $t_{\text{inititial}}$ of 30 s, Γ_{ZnPor} of 4.19 nmol·cm^{-2}, and $\Delta_o^w\phi_{\text{final}}$ of –0.25 V. **(b)** Current transients probing the influence of t_{initial} were obtained at a constant Γ_{ZnPor} of 4.19 nmol·cm^{-2}, $\Delta_o^w\phi_{\text{initial}}$ of +0.25 V, and $\Delta_o^w\phi_{\text{final}}$ of –0.25 V.

Supporting References

(1) Molina-Osorio, A. F.; Cheung, D.; O'Dwyer, C.; Stewart, A. A.; Dossot, M.; Herzog, G.; Scanlon, M. D. Self-Assembly of Porphyrin Nanostructures at the Interface between Two Immiscible Liquids. *J. Phys. Chem. C* **2020**, *124* (12), 6929–6937. https://doi.org/10.1021/acs.jpcc.0c00437.

(2) Smirnov, E.; Peljo, P.; Scanlon, M. D.; Girault, H. H. Gold Nanofilm Redox Catalysis for Oxygen Reduction at Soft Interfaces. *Electrochim. Acta* **2016**, *197*, 362–373. https://doi.org/10.1016/j.electacta.2015.10.104.

(3) Cherian, S.; Wamser, C. C. Adsorption and Photoactivity of Tetra(4-Carboxyphenyl)Porphyrin (TCPP) on Nanoparticulate TiO_2. *J. Phys. Chem. B* **2000**, *104* (15), 3624–3629. https://doi.org/10.1021/jp994459v.

(4) Cervera, J.; Gilabert, M. A.; Manzanares, J. A. Liquid-Vapor Coexistence and the PVT Surface of a Lattice Fluid. *Am. J. Phys.* **2011**, *79* (2), 206–213. https://doi.org/10.1119/1.3531942.

Reversible ion adsorption/exchange at interfacial soft porphyrin nanostructures

$c^{o,b}\ R_2\,N^+\ TB^- \mid\ c_{COO^-}, c_{COOH}, c_{C\,OOR_2\,N}, c_{R_2\,N^+}, c_{H^+}, c_{Li^+}, c_{TB^-}, c_{HCit^{2-}} \mid$
$pH^b\ ,\ c^{w,b}\ Li_2\ HCit^{2-}$

pHb bulk aqueous pH

Concentrations in mM = mol m^{-3} units

c0 : 1000 standard concentration
cHb = c0 10^{-pHb} : H^+ in bulk aqueous phase
cob : $R_2\,NTB$ in bulk organic phase
cwb : $Li_2\,HCit$ in bulk aqueous phase
cLib : Li^+ in bulk aqueous phase
cCOOT : total concentration of carboxyl groups in interfacial film
cR2NIN : $R_2\,N^+$ in interfacial film
cTBIN : TB^- in interfacial film
cLiIN : Li^+ in interfacial film
cHIN : H^+ in interfacial film
cHCitIN : $HCit^{2-}$ in interfacial film

Equilibrium constants

PR2N : $R_2\,N^+$ chemical partition equilibrium constant (for transfer o→IN)
PTB : TB^- chemical partition equilibrium constant (for transfer o→IN)
PH : H^+ chemical partition equilibrium constant (for transfer w→IN)
PLi : Li^+ chemical partition equilibrium constant (for transfer w→IN)
PHCit : $HCit^{2-}$ chemical partition equilibrium constant (for transfer w→IN)
Ka = 10^{-pKa} : carboxyl acid group dissociation constant (dimensionless)
KaIN = Ka PH : carboxyl acid group dissociation constant (dimensionless)
Kb = 10^{-pKb} : $R_2\,N^+$binding constant (mM^{-1})
KbIN = Kb/PR2N : $R_2\,N^+$binding constant in interfacial film (mM^{-1})
KieIN = KaIN KbIN c0 : ion-exchange constant in interfacial film (dimensionless)

LIN thickness of ZnPor-IN interfacial film (m)

$\Delta\phi$: $\Delta_o^w\,\phi$ applied interfacial Galvani potential (V)
f = F/(RT) (V^{-1})

y = Exp[-f (ϕ^{IN} - $\phi^{o,bulk}$)] auxiliary variable (obtained from solution local electroneutrality equation)

qo = F LIN (cR2NIN + cCOOR2N - cTBIN) (C m^{-2})
tabqo : List {$\Delta\phi$,qo,y} for $\Delta\phi$ varying from -0.3 to +0.05 at 0.001 increments

C = - 100 dqo/d$\Delta\phi$ (capacitance, evaluated as ratio of increments) (μF cm^{-2} = (F m^{-2})/100)
tabC : List {$\Delta\phi$, C}

ϵi : initial value of $\Delta\phi$ in scan (V)
ϵf : final value of $\Delta\phi$ in scan (V)
ν : scan rate (V/s)
t : time (s)

Rsol : solution resistance (MOhm cm^2, observe that V/(MOhm cm^2) = μA cm^{-2})

Rct : charge transfer resistance (MOhm cm^2, observe that μF cm^{-2} MOhm cm^2 = s)

ϵq[t] : potential drop across the film (V)

```
In[1380]:= (*Γ = 0.34 nmol cm^-2, 1 mV/s*)
(*Adjustable parameters*)
cCOOT = 42; pKb = 3.3; Rsol = .0045; Rct = 3.5; Pall = .0003;
(*Known data, fixed parameters and variable definitions*)
cwb = 10 ; cob = 5 ; pHb = 5.8; c0 = 10^3; cHb = c0 10^-pHb; cLib = 2 cwb - cHb;
LIN = 10^-7;
F = 96 485; R = 8.3144; T = 298; f = F / (R T) (*coherent SI units*);
PR2N = Pall; PTB = Pall; PH = Pall; PLi = Pall; PHCit = Pall;
pKa = 5.8; KaIN = 10^-pKa PH; KbIN = 10^-pKb / PR2N; KieIN = KaIN KbIN c0;
cR2NIN[y_] := PR2N cob y;
cTBIN[y_] := PTB cob / y;
cLiIN[y_, Δϕ_] := PLi cLib y Exp[f Δϕ ];
cHIN[y_, Δϕ_] := PH cHb y Exp[f Δϕ ];
cHCitIN[y_, Δϕ_] := PHCit cwb / (y Exp[f Δϕ ])^2;
(*Calculation of the film capacitance as
 a function of the potential drop across the film*)
Off[FindRoot::lstol];
Clear[Δϕ]; n = 1; Δϕi = -.3; δΔϕ = .001; Δϕf = .05; Δϕ = Δϕi;
tabqo = {{Δϕ, 0, Exp[-2 f Δϕ / 3 ] (2 cwb PHCit / (cob PR2N))^(1/3)}};
While[Δϕ < Δϕf + δΔϕ / 2,
   tabqo = Append[tabqo, {Δϕ, F LIN (cR2NIN[y] + cR2NIN[y] KieIN cCOOT /
             (KaIN c0 + cHIN[y, Δϕ] + KieIN cR2NIN[y]) - cTBIN[y]), y} /.
      FindRoot[cR2NIN[y] - cTBIN[y] + cLiIN[y, Δϕ] + cHIN[y, Δϕ] - 2 cHCitIN[y, Δϕ] -
         cCOOT KaIN c0 / (KaIN c0 + cHIN[y, Δϕ] + KieIN cR2NIN[y]) == 0,
        {y, tabqo[[n, 3]]}]]; Δϕ = Δϕi + δΔϕ n; n++];
tabC = Table[{tabqo[[i + 1, 1]], -100 ((tabqo[[i + 2, 2]] - tabqo[[i, 2]]) /
         (tabqo[[i + 2, 1]] - tabqo[[i, 1]]))}, {i, 2, Length[tabqo] - 2}];
Cint = Interpolation[tabC];
(*Equivalent circuit Rsol in series with parallel combination of C and Rct*)
ϵi = 0; ϵf = -.1965; ν = 10^-3; sol = NDSolve[
   {Cint[ϵq[t]] ϵq'[t] == (ϵf + ν Abs[(ϵi - ϵf) / ν - t] - ϵq[t]) / Rsol - ϵq[t] / Rct,
    ϵq[0] == 0}, ϵq, {t, 0, 2 (ϵi - ϵf) / ν}];
CV1sim = Show[{
     ParametricPlot[
      {ϵf + ν Abs[(ϵi - ϵf) / ν - t], ((ϵf + ν Abs[(ϵi - ϵf) / ν - t] - ϵq[t]) / Rsol) /. sol},
      {t, 0, 2 (ϵi - ϵf) / ν}, PlotStyle → Black, AspectRatio → 1 / GoldenRatio]}];

(*Γ = 0.88 nmol cm^-2, 1 mV/s*)
cCOOT = 100; pKb = 3.3; Rsol = .0045; Rct = 2; Pall = .0003;
PR2N = Pall; PTB = Pall; PH = Pall; PLi = Pall; PHCit = Pall;
KaIN = 10^-pKa PH; KbIN = 10^-pKb / PR2N; KieIN = KaIN KbIN c0;
(*Calculation of the film capacitance as
 a function of the potential drop across the film*)
Clear[Δϕ]; n = 1; Δϕ = Δϕi;
tabqo = {{Δϕ, 0, Exp[-2 f Δϕ / 3 ] (2 cwb PHCit / (cob PR2N))^(1/3)}};
While[Δϕ < Δϕf + δΔϕ / 2,
   tabqo = Append[tabqo, {Δϕ, F LIN (cR2NIN[y] + cR2NIN[y] KieIN
            cCOOT / (KaIN c0 + cHIN[y, Δϕ] + KieIN cR2NIN[y]) - cTBIN[y]), y} /.
      FindRoot[cR2NIN[y] - cTBIN[y] + cLiIN[y, Δϕ] + cHIN[y, Δϕ] - 2 cHCitIN[y, Δϕ] -
         cCOOT KaIN c0 / (KaIN c0 + cHIN[y, Δϕ] + KieIN cR2NIN[y]) == 0,
        {y, tabqo[[n, 3]]}]]; Δϕ = Δϕi + δΔϕ n; n++];
tabC = Table[{tabqo[[i + 1, 1]], -100 ((tabqo[[i + 2, 2]] - tabqo[[i, 2]]) /
        (tabqo[[i + 2, 1]] - tabqo[[i, 1]]))},
   {i, 2, Length[tabqo] - 2}]; Cint = Interpolation[tabC];
```

```
sol = NDSolve[{Cint[ϵq[t]] ϵq'[t] == (ϵf + ν Abs[(ϵi - ϵf) / ν - t] - ϵq[t]) / Rsol -
      ϵq[t] / Rct, ϵq[0] == 0}, ϵq, {t, 0, 2 (ϵi - ϵf) / ν}];
CV2sim = Show[{
    ParametricPlot[
     {ϵf + ν Abs[(ϵi - ϵf) / ν - t], ((ϵf + ν Abs[(ϵi - ϵf) / ν - t] - ϵq[t]) / Rsol) /. sol},
     {t, 0, 2 (ϵi - ϵf) / ν}, PlotStyle → Red, AspectRatio → 1 / GoldenRatio]}];

(*Γ = 1.94 nmol cm^−2, 1 mV/s*)
cCOOT = 214; pKb = 3.1; Rsol = .0028; Rct = 2; Pall = .0003;
PR2N = Pall; PTB = Pall; PH = Pall; PLi = Pall; PHCit = Pall;
KaIN = 10^-pKa PH; KbIN = 10^-pKb / PR2N; KieIN = KaIN KbIN c0;
(*Calculation of the film capacitance as
 a function of the potential drop across the film*)
Clear[Δϕ]; n = 1; Δϕ = Δϕi;
tabqo = {{Δϕ, 0, Exp[-2 f Δϕ / 3 ] (2 cwb PHCit / (cob PR2N)) ^ (1 / 3)}};
While[Δϕ < Δϕf + δΔϕ / 2,
  tabqo = Append[tabqo, {Δϕ, F LIN (cR2NIN[y] + cR2NIN[y] KieIN
          cCOOT / (KaIN c0 + cHIN[y, Δϕ] + KieIN cR2NIN[y]) - cTBIN[y]), y} /.
     FindRoot[cR2NIN[y] - cTBIN[y] + cLiIN[y, Δϕ] + cHIN[y, Δϕ] - 2 cHCitIN[y, Δϕ] -
        cCOOT KaIN c0 / (KaIN c0 + cHIN[y, Δϕ] + KieIN cR2NIN[y]) == 0,
      {y, tabqo[[n, 3]]}]]; Δϕ = Δϕi + δΔϕ n; n++];
tabC = Table[{tabqo[[i + 1, 1]], -100 ((tabqo[[i + 2, 2]] - tabqo[[i, 2]]) /
      (tabqo[[i + 2, 1]] - tabqo[[i, 1]]))},
  {i, 2, Length[tabqo] - 2}]; Cint = Interpolation[tabC];
sol = NDSolve[{Cint[ϵq[t]] ϵq'[t] == (ϵf + ν Abs[(ϵi - ϵf) / ν - t] - ϵq[t]) / Rsol -
      ϵq[t] / Rct, ϵq[0] == 0}, ϵq, {t, 0, 2 (ϵi - ϵf) / ν}];
CV3sim = Show[{
    ParametricPlot[
     {ϵf + ν Abs[(ϵi - ϵf) / ν - t], ((ϵf + ν Abs[(ϵi - ϵf) / ν - t] - ϵq[t]) / Rsol) /. sol},
     {t, 0, 2 (ϵi - ϵf) / ν}, PlotStyle → Blue, AspectRatio → 1 / GoldenRatio]}];

(*Γ = 4.19 nmol cm^−2, 1 mV/s*)
cCOOT = 416; pKb = 3.1; Rsol = .0014; Rct = 2; Pall = .0003;
PR2N = Pall; PTB = Pall; PH = Pall; PLi = Pall; PHCit = Pall;
KaIN = 10^-pKa PH; KbIN = 10^-pKb / PR2N; KieIN = KaIN KbIN c0;
(*Calculation of the film capacitance as
 a function of the potential drop across the film*)
Clear[Δϕ]; n = 1; Δϕ = Δϕi;
tabqo = {{Δϕ, 0, Exp[-2 f Δϕ / 3 ] (2 cwb PHCit / (cob PR2N)) ^ (1 / 3)}};
While[Δϕ < Δϕf + δΔϕ / 2,
  tabqo = Append[tabqo, {Δϕ, F LIN (cR2NIN[y] + cR2NIN[y] KieIN
          cCOOT / (KaIN c0 + cHIN[y, Δϕ] + KieIN cR2NIN[y]) - cTBIN[y]), y} /.
     FindRoot[cR2NIN[y] - cTBIN[y] + cLiIN[y, Δϕ] + cHIN[y, Δϕ] - 2 cHCitIN[y, Δϕ] -
        cCOOT KaIN c0 / (KaIN c0 + cHIN[y, Δϕ] + KieIN cR2NIN[y]) == 0,
      {y, tabqo[[n, 3]]}]]; Δϕ = Δϕi + δΔϕ n; n++];
tabC = Table[{tabqo[[i + 1, 1]], -100 ((tabqo[[i + 2, 2]] - tabqo[[i, 2]]) /
      (tabqo[[i + 2, 1]] - tabqo[[i, 1]]))},
  {i, 2, Length[tabqo] - 2}]; Cint = Interpolation[tabC];
sol = NDSolve[{Cint[ϵq[t]] ϵq'[t] == (ϵf + ν Abs[(ϵi - ϵf) / ν - t] - ϵq[t]) / Rsol -
      ϵq[t] / Rct, ϵq[0] == 0}, ϵq, {t, 0, 2 (ϵi - ϵf) / ν}];
CV4sim = Show[{
    ParametricPlot[
     {ϵf + ν Abs[(ϵi - ϵf) / ν - t], ((ϵf + ν Abs[(ϵi - ϵf) / ν - t] - ϵq[t]) / Rsol) /. sol},
     {t, 0, 2 (ϵi - ϵf) / ν}, PlotStyle → Magenta, AspectRatio → 1 / GoldenRatio]}];
```

(*Experimental CV data should be previously
 loaded as {V,μA cm^{-2}} lists CV1, CV2, CV3 and CV4.*)

```
FigA = Show[{CV1sim, CV2sim, CV3sim, CV4sim},
  Frame → True, FrameStyle → AbsoluteThickness[.9], FrameLabel →
   {Style["Δ^w_oϕ/V", 16, SingleLetterItalics → False], Style["j/(μA cm^-2)", 16]},
  AspectRatio → 1.3, AxesOrigin → {-.2, -6}, BaseStyle →
   {FontSize → 13, FontFamily → "Arial", AbsoluteThickness[1.4]}, Epilog →
   {PointSize → Small, Text[Style["(a)", 16, Bold], {-1.15 .2, -6 * .05 + 6 × .95}],
    Text["Γ_ZnPor/(nmol cm^-2)", {-.06, 5.5}, {0, 0}], Point[CV1],
    Line[{{-.06, 4.8}, {-.04, 4.8}}], Text["0.34", {-.035, 4.8}, {-1, 0}], Red,
    Point[CV2], Line[{{-.06, 4.2}, {-.04, 4.2}}], Text["0.88", {-.035, 4.2},
      {-1, 0}], Blue, Point[CV3], Line[{{-.06, 3.6}, {-.04, 3.6}}],
    Text["1.94", {-.035, 3.6}, {-1, 0}], Magenta, Point[CV4],
    Line[{{-.06, 3.}, {-.04, 3.}}], Text["4.19", {-.035, 3.}, {-1, 0}]},
  AspectRatio → 1.2, PlotRange → {{-.2, 0}, {-6, 6}},
  PlotRangeClipping → False, ImageSize → {Automatic, 350}]
```

Out[1425]=

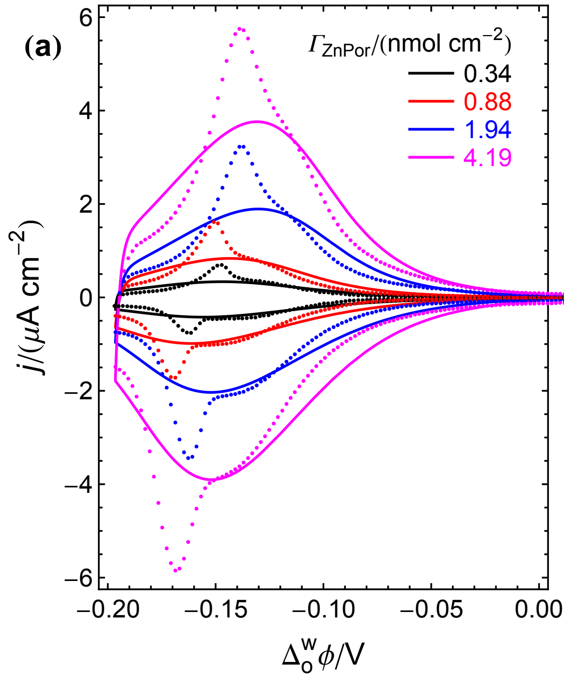

In[1426]:=

```
(*Γ = 0.34 nmol cm^−2, pH 5.8, 5 mV/s*)
(*Adjustable parameters*)
cCOOT = 42; pHb = 5.8;  pKb = 3.5; Rsol = .004; Rct = 3.; Pall = .0003;
cHb = c0 10^-pHb; cLib = 2 cwb - cHb;
PR2N = Pall; PTB = Pall; PH = Pall; PLi = Pall; PHCit = Pall;
KaIN = 10^-pKa PH; KbIN = 10^-pKb / PR2N; KieIN = KaIN KbIN c0;
(*Calculation of the film capacitance as
 a function of the potential drop across the film*)
Clear[Δϕ]; n = 1; Δϕ = Δϕi;
tabqo = {{Δϕ, 0, Exp[-2 f Δϕ / 3 ] (2 cwb PHCit / (cob PR2N)) ^ (1 / 3)}};
While[Δϕ < Δϕf + δΔϕ / 2,
  tabqo = Append[tabqo, {Δϕ, F LIN (cR2NIN[y] + cR2NIN[y] KieIN
          cCOOT / (KaIN c0 + cHIN[y, Δϕ] + KieIN cR2NIN[y]) - cTBIN[y]), y} /.
       FindRoot[cR2NIN[y] - cTBIN[y] + cLiIN[y, Δϕ] + cHIN[y, Δϕ] - 2 cHCitIN[y, Δϕ] -
          cCOOT KaIN c0 / (KaIN c0 + cHIN[y, Δϕ] + KieIN cR2NIN[y]) == 0,
         {y, tabqo[[n, 3]]}]]; Δϕ = Δϕi + δΔϕ n; n++];
tabC = Table[{tabqo[[i + 1, 1]], -100 ((tabqo[[i + 2, 2]] - tabqo[[i, 2]]) /
        (tabqo[[i + 2, 1]] - tabqo[[i, 1]]))},
```

Homogeneous membrane model for ZnPr-INs (Feb 10, 2020)

$c^{o,b}$ $R_2\,N^+\,TB^-$ | c_{COO^-}, c_{COOH}, c_{COOR_2N}, $c_{R_2N^+}$, c_{H^+}, c_{Li^+}, c_{TB^-}, $c_{HCit^{2-}}$ | pH^b , $c^{w,b}$ $Li_2\,HCit^{2-}$

```
(*Γ = 0.34 nmol cm^−2, 1 mV/s, Narrow peak*)
(*Adjustable parameters*)
cCOOT = 10; g = 3.5; pKb = 4.04; Rsol = .013; Rct = 7; Pall = .00003;
(*Known data, fixed parameters and variable definitions*)
cwb = 10 (*mol m^-3*); cob = 5 (*mol m^-3*);
LIN = 10^-7;
F = 96 485; R = 8.3144; T = 298; f = F / (R T); pHb = 5.8; cLib = 2 cwb - 10^(3 - pHb);
pKa = 5.8; KaIN = 10^-pKa PH; KieIN = 10^(3 - pKa - pKb) PH / PR2N;
PTB := Pall; PR2N := Pall; PH := Pall; PLi := Pall; PHCit := Pall; PCOO := 1;
cR2NIN[y_] := PR2N cob y; cTBIN[y_] := PTB cob / y;
cLiIN[y_, Δϕ_] := PLi cLib y Exp[f Δϕ];
cHCitIN[y_, Δϕ_] := PHCit cwb / (y Exp[f Δϕ])^2;
cHIN[y_, Δϕ_] := PH 10^(3 - pHb) y Exp[f Δϕ];
Clear[Δϕ]; n = 1; Δϕ0 = -.3005; Δϕ = Δϕ0;
table = {{Δϕ, 0, 0, Exp[-2 f Δϕ / 3] (2 cwb PHCit / (cob PR2N))^(1 / 3), 0, 0, 0, 0,
    0, 0, KieIN cR2NIN[Exp[-2 f Δϕ / 3] (2 cwb PHCit / (cob PR2N))^(1 / 3)] /
       (KieIN cR2NIN[Exp[-2 f Δϕ / 3] (2 cwb PHCit / (cob PR2N))^(1 / 3)] +
         cHIN[Exp[-2 f Δϕ / 3] (2 cwb PHCit / (cob PR2N))^(1 / 3), Δϕ] + KaIN 10^3)}};
Clear[x];(*y = Exp[-f (phiIN - phio,bulk)]*)
Off[FindRoot::lstol];
While[Δϕ < .01,
   table = Append[table, {Δϕ, -Log[y] / f, 100 (Log[y] / f / Δϕ + 1), y, cR2NIN[y],
        cHCitIN[y, Δϕ], cTBIN[y], cLiIN[y, Δϕ], cHIN[y, Δϕ] 10^-3,
        cCOOT θ Exp[-g θ] KaIN 10^3 / (KieIN cR2NIN[y]), θ} /.
      FindRoot[{cR2NIN[y] - cTBIN[y] + cLiIN[y, Δϕ] + cHIN[y, Δϕ] -
           2 cHCitIN[y, Δϕ] - cCOOT θ Exp[-g θ] KaIN 10^3 / (KieIN cR2NIN[y]) == 0,
         Exp[g θ] (1 - θ) / θ == (KaIN 10^3 + cHIN[y, Δϕ]) / (KieIN cR2NIN[y])},
        {{y, table[[n, 4]]}, {θ, table[[n, 11]]}}]]; Δϕ = Δϕ0 + .001 n; n++];
tabqo = Table[{table[[i, 1]], table[[i, 5]] - table[[i, 7]] + table[[i, 11]] cCOOT},
    {i, 2, Length[table]}];
tabC = Table[{tabqo[[i + 1, 1]], -100 F LIN ((tabqo[[i + 2, 2]] - tabqo[[i, 2]]) /
         (tabqo[[i + 2, 1]] - tabqo[[i, 1]]))}, {i, 2, Length[tabqo] - 2}];
Cint = Interpolation[tabC];
ϵi = 0; ϵf = -.1975; ν = 10^-3; solNarrow = NDSolve[
   {Cint[ϵq[t]] ϵq'[t] == (ϵf + ν Abs[(ϵi - ϵf) / ν - t] - ϵq[t]) / Rsol - ϵq[t] / Rct,
    ϵq[0] == 0}, ϵq, {t, 0, 2 (ϵi - ϵf) / ν}];
tableCV1NarrowSim = Table[{ϵf + ν Abs[(ϵi - ϵf) / ν - t],
     Part[((ϵf + ν Abs[(ϵi - ϵf) / ν - t] - ϵq[t]) / Rsol) /. solNarrow, 1]},
    {t, 0, 2 (ϵi - ϵf) / ν, 2 (ϵi - ϵf) / ν / 1000}];
(*Broad peak*)
(*Adjustable parameters*)
cCOOT = 31; g = 0.7; pKb = 3.3;
KieIN = 10^(3 - pKa - pKb) PH / PR2N; Clear[x];
Clear[Δϕ]; n = 1; Δϕ = Δϕ0;
table = {{Δϕ, 0, 0, Exp[-2 f Δϕ / 3] (2 cwb PHCit / (cob PR2N))^(1 / 3), 0, 0, 0, 0,
    0, 0, KieIN cR2NIN[Exp[-2 f Δϕ / 3] (2 cwb PHCit / (cob PR2N))^(1 / 3)] /
       (KieIN cR2NIN[Exp[-2 f Δϕ / 3] (2 cwb PHCit / (cob PR2N))^(1 / 3)] +
         cHIN[Exp[-2 f Δϕ / 3] (2 cwb PHCit / (cob PR2N))^(1 / 3), Δϕ] + KaIN 10^3)}};
While[Δϕ < .01, table = Append[table, {Δϕ, -Log[y] / f, 100 (Log[y] / f / Δϕ + 1) ,
```

```
       y, cR2NIN[y], cHCitIN[y, Δϕ], cTBIN[y], cLiIN[y, Δϕ],
       cHIN[y, Δϕ] 10^-3, cCOOT θ Exp[-g θ] KaIN 10^3 / (KieIN cR2NIN[y]), θ} /.
      FindRoot[{cR2NIN[y] - cTBIN[y] + cLiIN[y, Δϕ] + cHIN[y, Δϕ] -
          2 cHCitIN[y, Δϕ] - cCOOT θ Exp[-g θ] KaIN 10^3 / (KieIN cR2NIN[y]) == 0,
        Exp[g θ] (1 - θ) / θ == (KaIN 10^3 + cHIN[y, Δϕ]) / (KieIN cR2NIN[y])},
       {{y, table[[n, 4]]}, {θ, table[[n, 11]]}}]]; Δϕ = Δϕ0 + .001 n; n++];
tabqo = Table[{table[[i, 1]], table[[i, 5]] - table[[i, 7]] + table[[i, 11]] cCOOT},
   {i, 2, Length[table]}];
tabC = Table[{tabqo[[i + 1, 1]], -100 F LIN ((tabqo[[i + 2, 2]] - tabqo[[i, 2]]) /
       (tabqo[[i + 2, 1]] - tabqo[[i, 1]]))}, {i, 2, Length[tabqo] - 2}];
Cint = Interpolation[tabC];
solBroad = NDSolve[
   {Cint[ϵq[t]] ϵq'[t] == (ϵf + ν Abs[(ϵi - ϵf) / ν - t] - ϵq[t]) / Rsol - ϵq[t] / Rct,
    ϵq[0] == 0}, ϵq, {t, 0, 2 (ϵi - ϵf) / ν}];
tableCV1BroadSim = Table[{ϵf + ν Abs[(ϵi - ϵf) / ν - t],
    Part[((ϵf + ν Abs[(ϵi - ϵf) / ν - t] - ϵq[t]) / Rsol) /. solBroad, 1]},
   {t, 0, 2 (ϵi - ϵf) / ν, 2 (ϵi - ϵf) / ν / 1000}];
tableCV1BNSim = Table[{tableCV1BroadSim[[i, 1]], tableCV1BroadSim[[i, 2]] +
      tableCV1NarrowSim[[i, 2]]}, {i, 1, Length[tableCV1BroadSim]}];
(*Γ = 0.34 nmol cm^-2, 1 mV/s*)
Fig034 = Show[ListPlot[CV1, PlotStyle → {Gray, PointSize → .015},
    Epilog → {Black, Text["(a)", {-.185, -.85 * .1 + .8 × .9}],
      Text["ΓZnpor = 0.34 nmol cm^-2", {-.07, -.85 * .1 + .8 × .9}, {0, 0}]},
    Frame → True, FrameStyle → AbsoluteThickness[.9],
    FrameLabel → {Style["Δ^w_oϕ/V", 16, SingleLetterItalics → False],
      Style["j/(μA cm^-2)", 16]}, AspectRatio → 1 / GoldenRatio,
    BaseStyle → {FontSize → 13, FontFamily → "Arial", AbsoluteThickness[1.1]},
    PlotRange → {{-.2, 0}, {-.85, .8}}, ImageSize → {Automatic, 200}],
  ListPlot[tableCV1BNSim, Joined → True, PlotStyle → Black]]
```

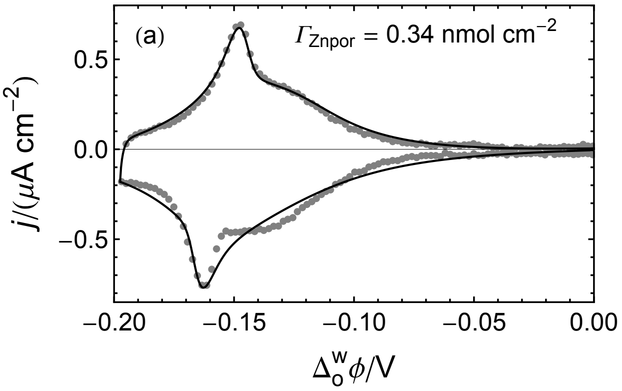

```
(*Γ = 0.88 nmol cm^-2, 1 mV/s, Narrow peak*)
(*Adjustable parameters*)
cCOOT = 24; g = 3.5; pKb = 4.13; Rsol = .008; Rct = 5; Pall = .00003;
(*Known data, fixed parameters and variable definitions*)
cwb = 10 (*mol m^-3*); cob = 5 (*mol m^-3*);
LIN = 10^-7;
F = 96 485; R = 8.3144; T = 298; f = F / (R T); pHb = 5.8; cLib = 2 cwb - 10^(3 - pHb);
pKa = 5.8; KaIN = 10^-pKa PH; KieIN = 10^(3 - pKa - pKb) PH / PR2N;
PTB := Pall; PR2N := Pall; PH := Pall; PLi := Pall; PHCit := Pall; PCOO := 1;
Clear[Δϕ]; n = 1; Δϕ0 = -.3005; Δϕ = Δϕ0;
table = {{Δϕ, 0, 0, Exp[-2 f Δϕ / 3] (2 cwb PHCit / (cob PR2N))^(1 / 3), 0, 0, 0, 0,
    0, 0, KieIN cR2NIN[Exp[-2 f Δϕ / 3] (2 cwb PHCit / (cob PR2N))^(1 / 3)] /
      (KieIN cR2NIN[Exp[-2 f Δϕ / 3] (2 cwb PHCit / (cob PR2N))^(1 / 3)] +
```

```
        cHIN[Exp[-2 f Δϕ / 3 ] (2 cwb PHCit / (cob PR2N)) ^ (1 / 3), Δϕ] + KaIN 10^3)}};
Clear[x];(*y = Exp[-f (phiIN - phio,bulk)]*)
cR2NIN[y_] := PR2N cob y; cTBIN[y_] := PTB cob / y;
cLiIN[y_, Δϕ_] := PLi cLib y Exp[f Δϕ ];
cHCitIN[y_, Δϕ_] := PHCit cwb / (y Exp[f Δϕ ]) ^2;
cHIN[y_, Δϕ_] := PH 10^ (3 - pHb) y Exp[f Δϕ ];
While[Δϕ < .01, table = Append[table, {Δϕ, -Log[y] / f, 100 (Log[y] / f / Δϕ + 1) ,
      y, cR2NIN[y], cHCitIN[y, Δϕ], cTBIN[y], cLiIN[y, Δϕ],
      cHIN[y, Δϕ] 10^-3, cCOOT θ Exp[-g θ] KaIN 10^3 / (KieIN cR2NIN[y]), θ} /.
    FindRoot[{cR2NIN[y] - cTBIN[y] + cLiIN[y, Δϕ] + cHIN[y, Δϕ] -
         2 cHCitIN[y, Δϕ] - cCOOT θ Exp[-g θ] KaIN 10^3 / (KieIN cR2NIN[y]) == 0,
       Exp[g θ] (1 - θ) / θ == (KaIN 10^3 + cHIN[y, Δϕ]) / (KieIN cR2NIN[y])},
      {{y, table[[n, 4]]}, {θ, table[[n, 11]]}}]]; Δϕ = Δϕ0 + .001 n; n++];
tabqo = Table[{table[[i, 1]], table[[i, 5]] - table[[i, 7]] + table[[i, 11]] cCOOT},
   {i, 2, Length[table]}];
tabC = Table[{tabqo[[i + 1, 1]], -100 F LIN ((tabqo[[i + 2, 2]] - tabqo[[i, 2]]) /
        (tabqo[[i + 2, 1]] - tabqo[[i, 1]]))}, {i, 2, Length[tabqo] - 2}];
Cint = Interpolation[tabC];
ϵi = 0; ϵf = -.1975; ν = 10^-3; solNarrow = NDSolve[
   {Cint[ϵq[t]] ϵq'[t] == (ϵf + ν Abs[(ϵi - ϵf) / ν - t] - ϵq[t]) / Rsol - ϵq[t] / Rct,
    ϵq[0] == 0}, ϵq, {t, 0, 2 (ϵi - ϵf) / ν}];
tableCV2NarrowSim = Table[{ϵf + ν Abs[(ϵi - ϵf) / ν - t],
     Part[((ϵf + ν Abs[(ϵi - ϵf) / ν - t] - ϵq[t]) / Rsol) /. solNarrow, 1]},
    {t, 0, 2 (ϵi - ϵf) / ν, 2 (ϵi - ϵf) / ν / 1000}];
(*Broad peak*)
(*Adjustable parameters*)
cCOOT = 70; g = 0.7; pKb = 3.4;
KieIN = 10^ (3 - pKa - pKb) PH / PR2N; Clear[x];
Clear[Δϕ]; n = 1; Δϕ0 = -.30005; Δϕ = Δϕ0;
table = {{Δϕ, 0, 0, Exp[-2 f Δϕ / 3 ] (2 cwb PHCit / (cob PR2N)) ^ (1 / 3), 0, 0, 0, 0,
    0, 0, KieIN cR2NIN[Exp[-2 f Δϕ / 3 ] (2 cwb PHCit / (cob PR2N)) ^ (1 / 3)] /
      (KieIN cR2NIN[Exp[-2 f Δϕ / 3 ] (2 cwb PHCit / (cob PR2N)) ^ (1 / 3)] +
        cHIN[Exp[-2 f Δϕ / 3 ] (2 cwb PHCit / (cob PR2N)) ^ (1 / 3), Δϕ] + KaIN 10^3)}};
(*y = Exp[-f (phiIN - phio,bulk)]*)
cR2NIN[y_] := PR2N cob y; cTBIN[y_] := PTB cob / y;
cLiIN[y_, Δϕ_] := PLi cLib y Exp[f Δϕ ];
cHCitIN[y_, Δϕ_] := PHCit cwb / (y Exp[f Δϕ ]) ^2;
cHIN[y_, Δϕ_] := PH 10^ (3 - pHb) y Exp[f Δϕ ];
While[Δϕ < .01, table = Append[table, {Δϕ, -Log[y] / f, 100 (Log[y] / f / Δϕ + 1) ,
      y, cR2NIN[y], cHCitIN[y, Δϕ], cTBIN[y], cLiIN[y, Δϕ],
      cHIN[y, Δϕ] 10^-3, cCOOT θ Exp[-g θ] KaIN 10^3 / (KieIN cR2NIN[y]), θ} /.
    FindRoot[{cR2NIN[y] - cTBIN[y] + cLiIN[y, Δϕ] + cHIN[y, Δϕ] -
         2 cHCitIN[y, Δϕ] - cCOOT θ Exp[-g θ] KaIN 10^3 / (KieIN cR2NIN[y]) == 0,
       Exp[g θ] (1 - θ) / θ == (KaIN 10^3 + cHIN[y, Δϕ]) / (KieIN cR2NIN[y])},
      {{y, table[[n, 4]]}, {θ, table[[n, 11]]}}]]; Δϕ = Δϕ0 + .001 n; n++];
tabqo = Table[{table[[i, 1]], table[[i, 5]] - table[[i, 7]] + table[[i, 11]] cCOOT},
   {i, 2, Length[table]}];
tabC = Table[{tabqo[[i + 1, 1]], -100 F LIN ((tabqo[[i + 2, 2]] - tabqo[[i, 2]]) /
        (tabqo[[i + 2, 1]] - tabqo[[i, 1]]))}, {i, 2, Length[tabqo] - 2}];
Cint = Interpolation[tabC];
ϵi = 0; ϵf = -.1975; solBroad = NDSolve[
   {Cint[ϵq[t]] ϵq'[t] == (ϵf + ν Abs[(ϵi - ϵf) / ν - t] - ϵq[t]) / Rsol - ϵq[t] / Rct,
    ϵq[0] == 0}, ϵq, {t, 0, 2 (ϵi - ϵf) / ν}];
tableCV2BroadSim = Table[{ϵf + ν Abs[(ϵi - ϵf) / ν - t],
     Part[((ϵf + ν Abs[(ϵi - ϵf) / ν - t] - ϵq[t]) / Rsol) /. solBroad, 1]},
    {t, 0, 2 (ϵi - ϵf) / ν, 2 (ϵi - ϵf) / ν / 1000}];
tableCV2BNSim = Table[{tableCV2BroadSim[[i, 1]], tableCV2BroadSim[[i, 2]] +
      tableCV2NarrowSim[[i, 2]]}, {i, 1, Length[tableCV1BroadSim]}];
```

```
(*Γ = 0.88 nmol cm^-2, 1 mV/s*)
Fig088 = Show[ListPlot[CV2, PlotStyle → {Gray, PointSize → .015},
    Epilog → {Black, Text["(b)", {-.185, -1.9 * .1 + 1.9 × .9}],
      Text["Γ_Znpor = 0.88 nmol cm^-2", {-.07, -1.9 * .1 + 1.9 × .9}, {0, 0}]},
    Frame → True, FrameStyle → AbsoluteThickness[.9],
    FrameLabel → {Style["Δ_o^wϕ/V", 16, SingleLetterItalics → False],
      Style["j/(μA cm^-2)", 16]}, AspectRatio → 1 / GoldenRatio,
    BaseStyle → {FontSize → 13, FontFamily → "Arial", AbsoluteThickness[1.1]},
    PlotRange → {{-.2, 0}, {-1.9, 1.9}}, ImageSize → {Automatic, 200}],
  ListPlot[tableCV2BNSim, Joined → True, PlotStyle → Black]]
```

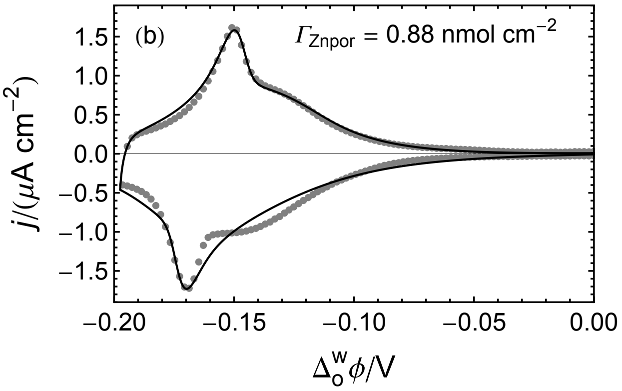

```
(*Γ = 1.94 nmol cm^-2, 1 mV/s, Narrow peak*)
(*Adjustable parameters*)
cCOOT = 46; g = 3.5; pKb = 3.98; Rsol = .0054; Rct = 4; Pall = .00003;
(*Known data, fixed parameters and variable definitions*)
cwb = 10 (*mol m^-3*); cob = 5 (*mol m^-3*);
LIN = 10^-7;
F = 96 485; R = 8.3144; T = 298; f = F / (R T); pHb = 5.8; cLib = 2 cwb - 10^(3 - pHb);
pKa = 5.8; KaIN = 10^-pKa PH; KieIN = 10^(3 - pKa - pKb) PH / PR2N;
PTB := Pall; PR2N := Pall; PH := Pall; PLi := Pall; PHCit := Pall; PCOO := 1;
Clear[Δϕ]; n = 1; Δϕ0 = -.3005; Δϕ = Δϕ0;
table = {{Δϕ, 0, 0, Exp[-2 f Δϕ / 3] (2 cwb PHCit / (cob PR2N))^(1 / 3), 0, 0, 0, 0,
    0, 0, KieIN cR2NIN[Exp[-2 f Δϕ / 3] (2 cwb PHCit / (cob PR2N))^(1 / 3)] /
      (KieIN cR2NIN[Exp[-2 f Δϕ / 3] (2 cwb PHCit / (cob PR2N))^(1 / 3)] +
        cHIN[Exp[-2 f Δϕ / 3] (2 cwb PHCit / (cob PR2N))^(1 / 3), Δϕ] + KaIN 10^3)}};
Clear[x];(*y = Exp[-f (phiIN - phio,bulk)]*)
cR2NIN[y_] := PR2N cob y; cTBIN[y_] := PTB cob / y;
cLiIN[y_, Δϕ_] := PLi cLib y Exp[f Δϕ];
cHCitIN[y_, Δϕ_] := PHCit cwb / (y Exp[f Δϕ])^2;
cHIN[y_, Δϕ_] := PH 10^(3 - pHb) y Exp[f Δϕ];
While[Δϕ < .01, table = Append[table, {Δϕ, -Log[y] / f, 100 (Log[y] / f / Δϕ + 1) ,
      y, cR2NIN[y], cHCitIN[y, Δϕ], cTBIN[y], cLiIN[y, Δϕ],
      cHIN[y, Δϕ] 10^-3, cCOOT θ Exp[-g θ] KaIN 10^3 / (KieIN cR2NIN[y]), θ} /.
     FindRoot[{cR2NIN[y] - cTBIN[y] + cLiIN[y, Δϕ] + cHIN[y, Δϕ] -
          2 cHCitIN[y, Δϕ] - cCOOT θ Exp[-g θ] KaIN 10^3 / (KieIN cR2NIN[y]) == 0,
        Exp[g θ] (1 - θ) / θ == (KaIN 10^3 + cHIN[y, Δϕ]) / (KieIN cR2NIN[y])},
      {{y, table[[n, 4]]}, {θ, table[[n, 11]]}}]]; Δϕ = Δϕ0 + .001 n; n++];
tabqo = Table[{table[[i, 1]], table[[i, 5]] - table[[i, 7]] + table[[i, 11]] cCOOT},
   {i, 2, Length[table]}];
tabC = Table[{tabqo[[i + 1, 1]], -100 F LIN ((tabqo[[i + 2, 2]] - tabqo[[i, 2]]) /
        (tabqo[[i + 2, 1]] - tabqo[[i, 1]]))}, {i, 2, Length[tabqo] - 2}];
Cint = Interpolation[tabC];
ϵi = 0; ϵf = -.1975; ν = 10^-3; solNarrow = NDSolve[
```

```
   {Cint[ϵq[t]] ϵq'[t] == (ϵf + ν Abs[(ϵi - ϵf) / ν - t] - ϵq[t]) / Rsol - ϵq[t] / Rct,
    ϵq[0] == 0}, ϵq, {t, 0, 2 (ϵi - ϵf) / ν}];
tableCV3NarrowSim = Table[{ϵf + ν Abs[(ϵi - ϵf) / ν - t],
     Part[((ϵf + ν Abs[(ϵi - ϵf) / ν - t] - ϵq[t]) / Rsol) /. solNarrow, 1]},
    {t, 0, 2 (ϵi - ϵf) / ν, 2 (ϵi - ϵf) / ν / 1000}];
(*Broad peak*)
(*Adjustable parameters*)
cCOOT = 160; g = 0.7; pKb = 3.2;
KieIN = 10^(3 - pKa - pKb) PH / PR2N; Clear[x];
Clear[Δϕ]; n = 1; Δϕ0 = -.30005; Δϕ = Δϕ0;
table = {{Δϕ, 0, 0, Exp[-2 f Δϕ / 3 ] (2 cwb PHCit / (cob PR2N))^(1 / 3), 0, 0, 0, 0,
    0, 0, KieIN cR2NIN[Exp[-2 f Δϕ / 3 ] (2 cwb PHCit / (cob PR2N))^(1 / 3)] /
      (KieIN cR2NIN[Exp[-2 f Δϕ / 3 ] (2 cwb PHCit / (cob PR2N))^(1 / 3)] +
        cHIN[Exp[-2 f Δϕ / 3 ] (2 cwb PHCit / (cob PR2N))^(1 / 3), Δϕ] + KaIN 10^3)}};
(*y = Exp[-f (phiIN - phio,bulk)]*)
cR2NIN[y_] := PR2N cob y; cTBIN[y_] := PTB cob / y;
cLiIN[y_, Δϕ_] := PLi cLib y Exp[f Δϕ ];
cHCitIN[y_, Δϕ_] := PHCit cwb / (y Exp[f Δϕ ])^2;
cHIN[y_, Δϕ_] := PH 10^(3 - pHb) y Exp[f Δϕ ];
While[Δϕ < .01, table = Append[table, {Δϕ, -Log[y] / f, 100 (Log[y] / f / Δϕ + 1) ,
      y, cR2NIN[y], cHCitIN[y, Δϕ], cTBIN[y], cLiIN[y, Δϕ],
      cHIN[y, Δϕ] 10^-3, cCOOT θ Exp[-g θ] KaIN 10^3 / (KieIN cR2NIN[y]), θ} /.
     FindRoot[{cR2NIN[y] - cTBIN[y] + cLiIN[y, Δϕ] + cHIN[y, Δϕ] -
         2 cHCitIN[y, Δϕ] - cCOOT θ Exp[-g θ] KaIN 10^3 / (KieIN cR2NIN[y]) == 0,
       Exp[g θ] (1 - θ) / θ == (KaIN 10^3 + cHIN[y, Δϕ]) / (KieIN cR2NIN[y])},
      {{y, table[[n, 4]]}, {θ, table[[n, 11]]}}]]; Δϕ = Δϕ0 + .001 n; n++];
tabqo = Table[{table[[i, 1]], table[[i, 5]] - table[[i, 7]] + table[[i, 11]] cCOOT},
    {i, 2, Length[table]}];
tabC = Table[{tabqo[[i + 1, 1]], -100 F LIN ((tabqo[[i + 2, 2]] - tabqo[[i, 2]]) /
        (tabqo[[i + 2, 1]] - tabqo[[i, 1]]))}, {i, 2, Length[tabqo] - 2}];
Cint = Interpolation[tabC];
ϵi = 0; ϵf = -.1975; solBroad = NDSolve[
   {Cint[ϵq[t]] ϵq'[t] == (ϵf + ν Abs[(ϵi - ϵf) / ν - t] - ϵq[t]) / Rsol - ϵq[t] / Rct,
    ϵq[0] == 0}, ϵq, {t, 0, 2 (ϵi - ϵf) / ν}];
tableCV3BroadSim = Table[{ϵf + ν Abs[(ϵi - ϵf) / ν - t],
     Part[((ϵf + ν Abs[(ϵi - ϵf) / ν - t] - ϵq[t]) / Rsol) /. solBroad, 1]},
    {t, 0, 2 (ϵi - ϵf) / ν, 2 (ϵi - ϵf) / ν / 1000}];
tableCV3BNSim = Table[{tableCV3BroadSim[[i, 1]], tableCV3BroadSim[[i, 2]] +
      tableCV3NarrowSim[[i, 2]]}, {i, 1, Length[tableCV1BroadSim]}];
(*Γ = 1.94 nmol cm^-2, 1 mV/s*)
Fig194 = Show[ListPlot[CV3, PlotStyle → {Gray, PointSize → .015},
    Epilog → {Black, Text["(c)", {-.185, -3.9 * .1 + 3.9 × .9}],
      Text["ΓZnpor = 1.94 nmol cm-2", {-.067, -3.9 * .1 + 3.9 × .9}, {0, 0}]},
    Frame → True, FrameStyle → AbsoluteThickness[.9],
    FrameLabel → {Style["Δowϕ/V", 16, SingleLetterItalics → False],
      Style["j/(μA cm-2)", 16]}, AspectRatio → 1 / GoldenRatio,
    BaseStyle → {FontSize → 13, FontFamily → "Arial", AbsoluteThickness[1.1]},
    PlotRange → {{-.2, 0}, {-3.9, 3.9}}, ImageSize → {Automatic, 200}],
   ListPlot[tableCV3BNSim, Joined → True, PlotStyle → Black]]
```

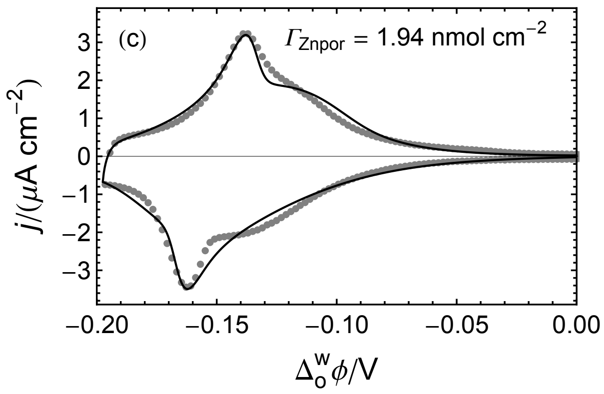

```
(*Γ = 4.19 nmol cm^−2, 1 mV/s, Narrow peak*)
(*Adjustable parameters*)
cCOOT = 84; g = 3.5; pKb = 4.05; Rsol = .0037; Rct = 10; Pall = .00003;
(*Known data, fixed parameters and variable definitions*)
cwb = 10 (*mol m^-3*); cob = 5 (*mol m^-3*);
LIN = 10^-7;
F = 96 485; R = 8.3144; T = 298; f = F / (R T); pHb = 5.8; cLib = 2 cwb - 10^(3 - pHb);
pKa = 5.8; KaIN = 10^-pKa PH; KieIN = 10^(3 - pKa - pKb) PH / PR2N;
PTB := Pall; PR2N := Pall; PH := Pall; PLi := Pall; PHCit := Pall; PCOO := 1;
Clear[Δϕ]; n = 1; Δϕ0 = -.3005; Δϕ = Δϕ0;
table = {{Δϕ, 0, 0, Exp[-2 f Δϕ / 3 ] (2 cwb PHCit / (cob PR2N)) ^ (1 / 3), 0, 0, 0, 0,
    0, 0, KieIN cR2NIN[Exp[-2 f Δϕ / 3 ] (2 cwb PHCit / (cob PR2N)) ^ (1 / 3)] /
       (KieIN cR2NIN[Exp[-2 f Δϕ / 3 ] (2 cwb PHCit / (cob PR2N)) ^ (1 / 3)] +
         cHIN[Exp[-2 f Δϕ / 3 ] (2 cwb PHCit / (cob PR2N)) ^ (1 / 3), Δϕ] + KaIN 10^3)}};
Clear[x];(*y = Exp[-f (phiIN - phio,bulk)]*)
cR2NIN[y_] := PR2N cob y; cTBIN[y_] := PTB cob / y;
cLiIN[y_, Δϕ_] := PLi cLib y Exp[f Δϕ ];
cHCitIN[y_, Δϕ_] := PHCit cwb / (y Exp[f Δϕ ]) ^2;
cHIN[y_, Δϕ_] := PH 10^(3 - pHb) y Exp[f Δϕ ];
While[Δϕ < .01, table = Append[table, {Δϕ, -Log[y] / f, 100 (Log[y] / f / Δϕ + 1) ,
       y, cR2NIN[y], cHCitIN[y, Δϕ], cTBIN[y], cLiIN[y, Δϕ],
       cHIN[y, Δϕ] 10^-3, cCOOT θ Exp[-g θ] KaIN 10^3 / (KieIN cR2NIN[y]), θ} /.
     FindRoot[{cR2NIN[y] - cTBIN[y] + cLiIN[y, Δϕ] + cHIN[y, Δϕ] -
          2 cHCitIN[y, Δϕ] - cCOOT θ Exp[-g θ] KaIN 10^3 / (KieIN cR2NIN[y]) == 0,
        Exp[g θ] (1 - θ) / θ == (KaIN 10^3 + cHIN[y, Δϕ]) / (KieIN cR2NIN[y])},
       {{y, table[[n, 4]]}, {θ, table[[n, 11]]}}]]]; Δϕ = Δϕ0 + .001 n; n++];
tabqo = Table[{table[[i, 1]], table[[i, 5]] - table[[i, 7]] + table[[i, 11]] cCOOT},
    {i, 2, Length[table]}];
tabC = Table[{tabqo[[i + 1, 1]], -100 F LIN ((tabqo[[i + 2, 2]] - tabqo[[i, 2]]) /
          (tabqo[[i + 2, 1]] - tabqo[[i, 1]]))}, {i, 2, Length[tabqo] - 2}];
Cint = Interpolation[tabC];
ϵi = 0; ϵf = -.1975; ν = 10^-3; solNarrow = NDSolve[
   {Cint[ϵq[t]] ϵq'[t] == (ϵf + ν Abs[(ϵi - ϵf) / ν - t] - ϵq[t]) / Rsol - ϵq[t] / Rct,
    ϵq[0] == 0}, ϵq, {t, 0, 2 (ϵi - ϵf) / ν}];
tableCV4NarrowSim = Table[{ϵf + ν Abs[(ϵi - ϵf) / ν - t],
     Part[((ϵf + ν Abs[(ϵi - ϵf) / ν - t] - ϵq[t]) / Rsol) /. solNarrow, 1]},
    {t, 0, 2 (ϵi - ϵf) / ν, 2 (ϵi - ϵf) / ν / 1000}];
(*Broad peak*)
(*Adjustable parameters*)
cCOOT = 295; g = 0.7; pKb = 3.2;
KieIN = 10^(3 - pKa - pKb) PH / PR2N; Clear[x];
Clear[Δϕ]; n = 1; Δϕ0 = -.30005; Δϕ = Δϕ0;
table = {{Δϕ, 0, 0, Exp[-2 f Δϕ / 3 ] (2 cwb PHCit / (cob PR2N)) ^ (1 / 3), 0, 0, 0, 0,
    0, 0, KieIN cR2NIN[Exp[-2 f Δϕ / 3 ] (2 cwb PHCit / (cob PR2N)) ^ (1 / 3)] /
```

```
      (KieIN cR2NIN[Exp[-2 f Δϕ / 3 ] (2 cwb PHCit / (cob PR2N)) ^ (1 / 3)] +
        cHIN[Exp[-2 f Δϕ / 3 ] (2 cwb PHCit / (cob PR2N)) ^ (1 / 3), Δϕ] + KaIN 10 ^ 3)}};
(*y = Exp[-f  (phiIN - phio,bulk)]*)
cR2NIN[y_] := PR2N cob y; cTBIN[y_] := PTB cob / y;
cLiIN[y_, Δϕ_] := PLi cLib y Exp[f Δϕ ];
cHCitIN[y_, Δϕ_] := PHCit cwb / (y Exp[f Δϕ ]) ^ 2;
cHIN[y_, Δϕ_] := PH 10 ^ (3 - pHb) y Exp[f Δϕ ];
While[Δϕ < .01, table = Append[table, {Δϕ, -Log[y] / f, 100 (Log[y] / f / Δϕ + 1) ,
      y, cR2NIN[y], cHCitIN[y, Δϕ], cTBIN[y], cLiIN[y, Δϕ],
      cHIN[y, Δϕ] 10 ^ - 3, cCOOT θ Exp[-g θ] KaIN 10 ^ 3 / (KieIN cR2NIN[y]), θ} /.
     FindRoot[{cR2NIN[y] - cTBIN[y] + cLiIN[y, Δϕ] + cHIN[y, Δϕ] -
         2 cHCitIN[y, Δϕ] - cCOOT θ Exp[-g θ] KaIN 10 ^ 3 / (KieIN cR2NIN[y]) == 0,
       Exp[g θ] (1 - θ) / θ == (KaIN 10 ^ 3 + cHIN[y, Δϕ]) / (KieIN cR2NIN[y])},
      {{y, table[[n, 4]]}, {θ, table[[n, 11]]}}]]; Δϕ = Δϕ0 + .001 n; n++];
tabqo = Table[{table[[i, 1]], table[[i, 5]] - table[[i, 7]] + table[[i, 11]] cCOOT},
    {i, 2, Length[table]}];
tabC = Table[{tabqo[[i + 1, 1]], -100 F LIN ((tabqo[[i + 2, 2]] - tabqo[[i, 2]]) /
        (tabqo[[i + 2, 1]] - tabqo[[i, 1]]))}, {i, 2, Length[tabqo] - 2}];
Cint = Interpolation[tabC];
ϵi = 0; ϵf = - .1975; solBroad = NDSolve[
   {Cint[ϵq[t]] ϵq '[t] == (ϵf + ν Abs[(ϵi - ϵf) / ν - t] - ϵq[t]) / Rsol - ϵq[t] / Rct,
    ϵq[0] == 0}, ϵq, {t, 0, 2 (ϵi - ϵf) / ν}];
tableCV4BroadSim = Table[{ϵf + ν Abs[(ϵi - ϵf) / ν - t],
     Part[((ϵf + ν Abs[(ϵi - ϵf) / ν - t] - ϵq[t]) / Rsol) /. solBroad, 1]},
    {t, 0, 2 (ϵi - ϵf) / ν, 2 (ϵi - ϵf) / ν / 1000}];
tableCV4BNSim = Table[{tableCV4BroadSim[[i, 1]], tableCV4BroadSim[[i, 2]] +
      tableCV4NarrowSim[[i, 2]]}, {i, 1, Length[tableCV1BroadSim]}];
(*Γ = 4.19 nmol cm^−2, 1 mV/s*)
Fig419 = Show[ListPlot[CV4, PlotStyle → {Gray, PointSize → .015},
    Epilog → {Black, Text["(d)", {- .185, -6.5 * .1 + 6.5 × .9}],
      Text["ΓZnpor = 4.19 nmol cm^-2", {- .067, -6.5 * .08 + 6.5 × .92}, {0, 0}]},
    Frame → True, FrameStyle → AbsoluteThickness[.9],
    FrameLabel → {Style["Δ^w_oϕ/V", 16, SingleLetterItalics → False],
      Style["j/(μA cm^-2)", 16]}, AspectRatio → 1 / GoldenRatio,
    BaseStyle → {FontSize → 13, FontFamily → "Arial", AbsoluteThickness[1.1]},
    PlotRange → {{- .2, 0}, {-6.5, 6.5}}, ImageSize → {Automatic, 200}],
  ListPlot[tableCV4BNSim, Joined → True, PlotStyle → Black]]
```

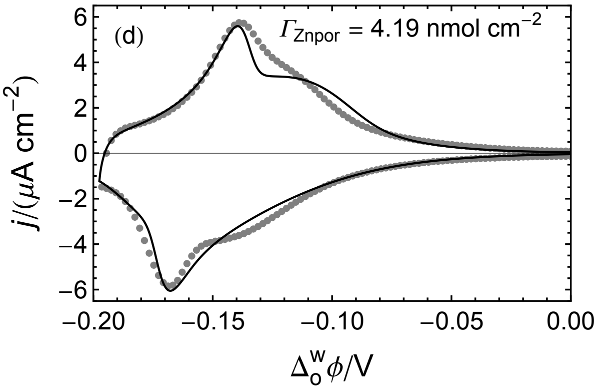

```
Grid[{{Fig034, Fig088}, {Fig194, Fig419}}, Spacings → 0, Alignment → Center]
```